JOURNAL
OF
GEOMAGNETISM
AND
GEOELECTRICITY

VOL. V NO. 3

SOCIETY
OF
TERRESTRIAL MAGNETISM AND ELECTRICITY
OF
JAPAN

NOV. 1953
KYOTO

JOURNAL OF GEOMAGNETISM AND GEOELECTRICITY

EDITORIAL OFFICE: Society of Terrestrial Magnetism and Electricity of Japan,
Geophysical Institute, Kyoto University, Kyoto, Japan

The fields of interest of this quarterly Journal are as follows:

Terrestrial Magnetism	Aurora and Night Sky
Atmospheric Electricity	The Ozone Layer
The Ionosphere	Physical States of the Upper Atmosphere
Radio Wave Propagation	Solar Phenomena relating to the above Subjects
Cosmic Rays	Electricity within the Earth

The text should be written in English, German or French. The price is provisionally set as 1 dollar per copy subject to change. We hope to exchange this Journal with periodical publications of any kind in the field of natural science.

The Editors

Anomalous Relations between H and Z Components of Transient Geomagnetic Variations*

By Tsuneji RIKITAKE and Izumi YOKOYAMA

(Earthquake Research Institute, Tokyo University)

Abstract

This is to summarize the writers' studies on the anomalous behavior of geomagnetic variations in Japan which were published in a series of papers in the Bulletin of the Earthquake Research Institute [1]. An anomalously large amplitude of the vertical component of geomagnetic variations is pointed out at Hermanus, S.A., and some observatories in Japan. The distribution especially in Japan is statistically examined. The anomaly is found in a limited area in the central part of Japan. The results of the analysis based on the potential theory show that the anomaly is caused by the magnetic field originating in the earth. The anomaly is well approximated by an apparent magnetic dipole situated under central Japan. But it still remains unknown why such a localized anomaly occurs on occasions of geomagnetic variation.

1. *Introduction.*

The vertical component (ΔZ) of geomagnetic variations of short period is generally small compared to the horizontal component (ΔH) as we can see on magnetograms from various observatories. In some places, however, we find an

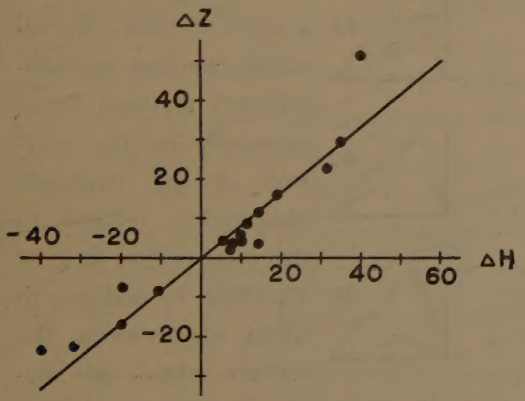

Fig. 1 The relation between ΔZ and ΔH for short period variations during the magnetic storm on Aug. 3, 1949 at Hermanus.

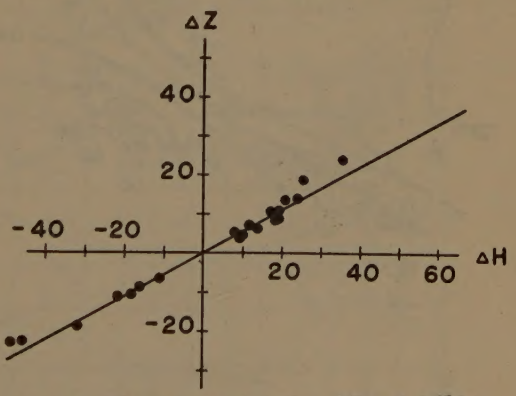

Fig. 2 The relation between ΔZ and ΔH for short period variations during the magnetic storm on Aug. 3, 1949 at Kakioka.

---

* Dedicated to Professor M. Hasegawa on his sixtieth birthday. The writers are greatly obliged to him for his ingenious method of graphical integration which is used in this paper.

anomalously large ΔZ. For instance $\Delta Z/\Delta H$ amounts to as much as 0.83 on an average at Hermanus Magnetic Observatory, South Africa, a remarkable parallelism between H and Z-curves being also observed there. The relation between ΔZ and ΔH at Hermanus is illustrated in Fig. 1 with respect to the variations during a magnetic storm that occurred on Aug. 3, 1949. Meanwhile $\Delta Z/\Delta H$ amounts to 0.56 on an average at Kakioka Magnetic Observatory, Japan as also shown in Fig. 2 for the same storm. According to the writers' detailed investigations [1] concerning the distribution of $\Delta Z/\Delta H$ in Japan, the fact that the anomalous behavior of geomagnetic variations is confined to the central part of Japan has been clarified. The shape of Z-curves observed at a station along the coast of the Japan Sea, only 200 *km* distant from Kakioka, is quite different from those observed at Kakioka. Even the sign of ΔZ reverses at stations in the northern part of Japan, while ΔH seems to be fairly regular throughout the country. The purpose of this paper is to study the anomalous behavior of geomagnetic variations and its possible cause by summarizing the various studies in the writers' previous papers [1].

2. *The distribution of $\Delta Z/\Delta H$ in Japan.*

In order to bring out more clearly the anomalous characteristics of geomagnetic variations in Japan, the writers collected magnetograms from permanent and temporary observatories in Japan and its vicinity. Fortunately we had well-distributed stations there, especially on the occasion of the magnetic observation related to the solar eclipse on June 19, 1936. In addition to those observations the writers added two stations for continuous recording of three geomagnetic components at Aburatsubo (139°37′E, 35°09′N) and Maze (138°48′E, 37°44′N). Although the periods of these observations are not the same, the characteristics of geomagnetic variation seem to be nearly

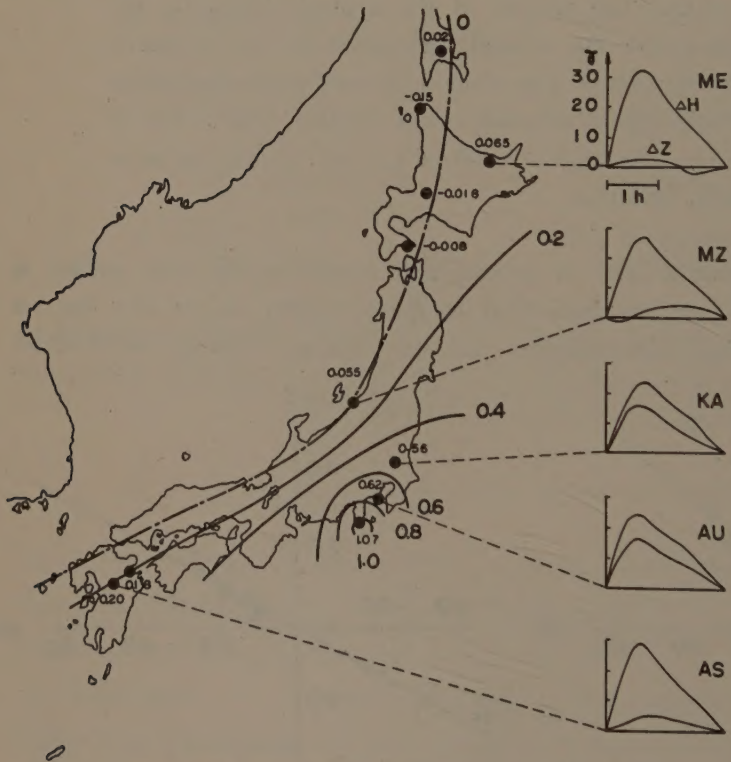

Fig. 3 The distribution of the statistical value of $\Delta Z/\Delta H$ in Japan. The variations in H and Z components at the time of the bay at 23 *h* on Sept. 11, 1952 are also illustrated for respective stations.

invariable. Hence we may construct a chart in which the distribution of the statistical values of $\Delta Z/\Delta H$ are illustrated as shown in Fig. 3. In the figure, the records of a geomagnetic bay that occurred at $23h$ on Sept. 11, 1952 are also shown for respective stations. We can clearly see that the amplitude of ΔZ is very large near the central part of Japan. The writers have never heard of such a strange distribution of geomagnetic variation except for the opposition of sign of ΔZ in British Isles and Western Europe [2].

3. *Anomalous geomagnetic fields originating within the earth.*

As the first step in clarifying the origin of the strange distribution mentioned above the writers intended to separate geomagnetic changes for each station into the parts originating outside and inside the earth. Since we had many temporary stations in and around Japan at the time of the solar eclipse on June 19, 1936, the writers collected copies of magnetograms of the magnetic storm that occurred with a SC at $9h\ 41m$ on June 18 from various observatories all over the earth. On the basis of these data the writers calculated the distribution of magnetic potential W for the SC and a remarkable change that occurred at $5h\ 50m$ GMT on June 19. The method of the graphical integration which was devised by M. Hasegawa and M. Ôta [3] was used in the calculation. The equi-potential lines are respectively illustrated in Figs. 4 and 5 together with the equivalent overhead current arrows. Combining the distribu-

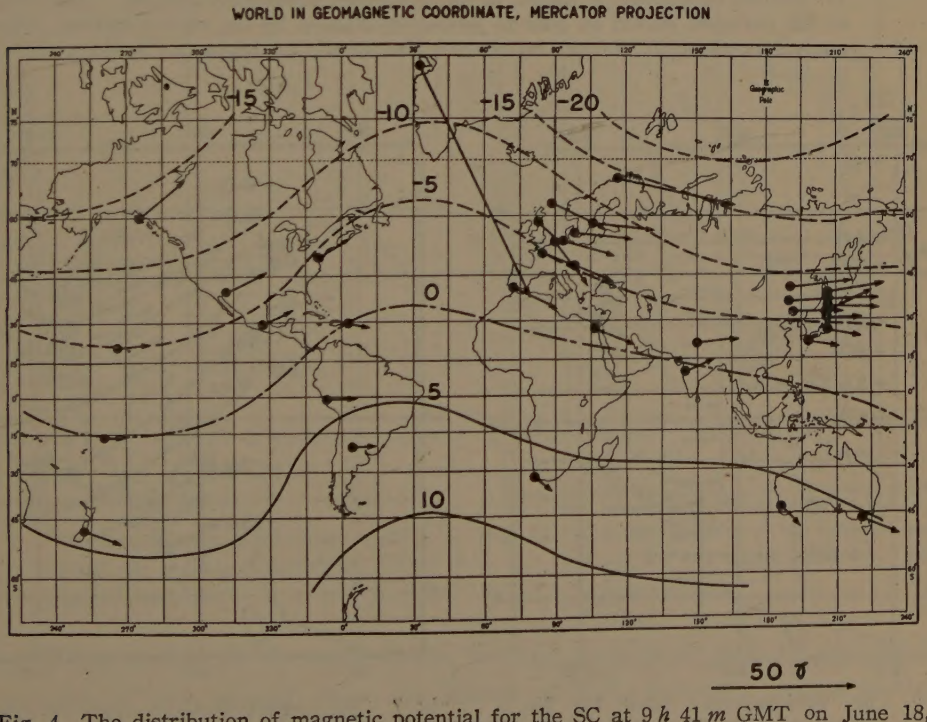

Fig. 4 The distribution of magnetic potential for the SC at $9h\ 41m$ GMT on June 18, 1936 as calculated by means of the graphical integration method. The unit of the potential should be read in *gamma* multiplied by the earth's radius. The equivalent overhead current arrows are also shown for respective stations.

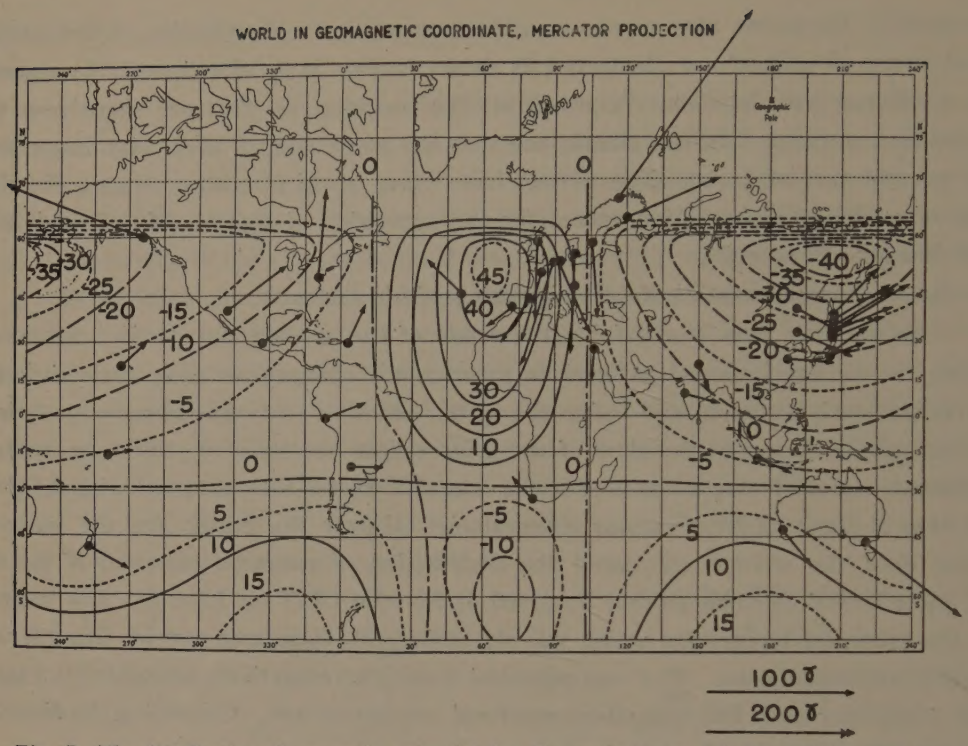

Fig. 5 The distribution of magnetic potential for the variation at 5 *h* 50 *m* GMT on June 19, 1936 as calculated by means of the graphical integration method. The unit of the potential should be read in *gamma* multiplied by the earth's radius. The equivalent overhead current arrows are also shown for respective stations.

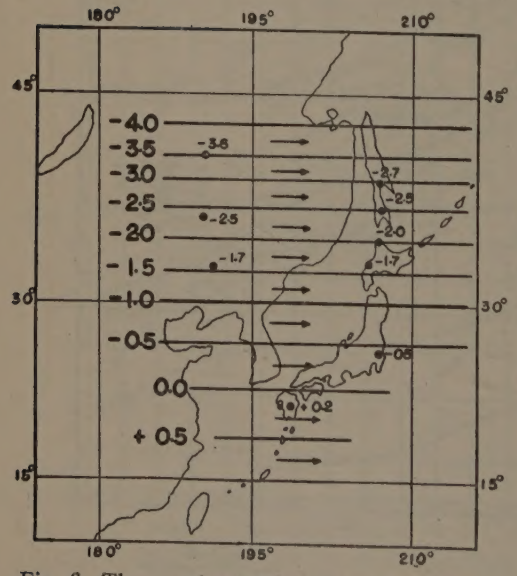

Fig. 6 The equi-potential lines for the external origin part of the magnetic potential for the SC. The unit is *gamma* multiplied by the earth's radius.

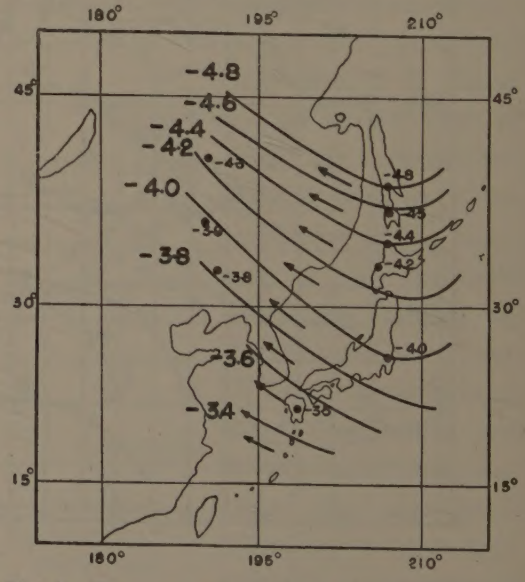

Fig. 7 The equi-potential lines for the internal origin part of the magnetic potential for the SC. The unit is *gamma* multiplied by the earth's radius.

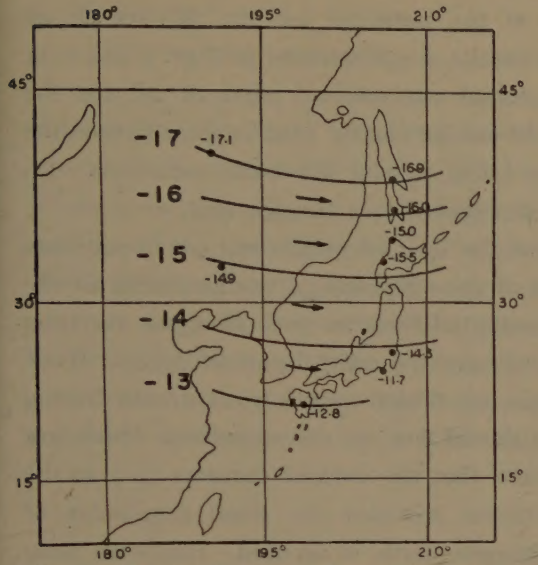

Fig. 8 The distribution of the external part of the magnetic potential for the variation at 5 *h* 50 *m* GMT on June 19, 1936. The unit is *gamma* multiplied by the earth's radius.

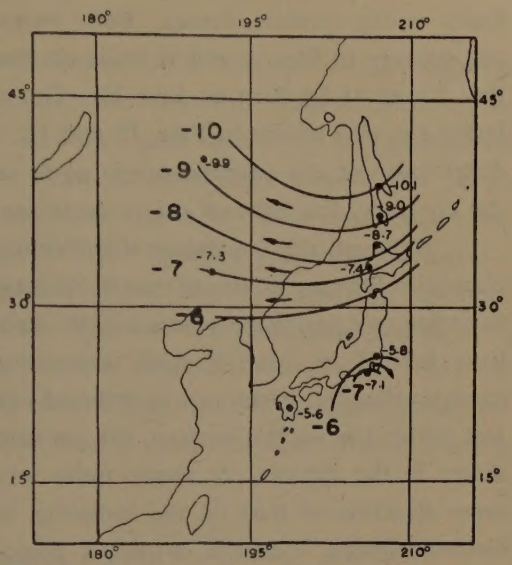

Fig. 9 The distribution of the internal part of the magnetic potential for the same variation. The unit is *gamma* multiplied by the earth's radius.

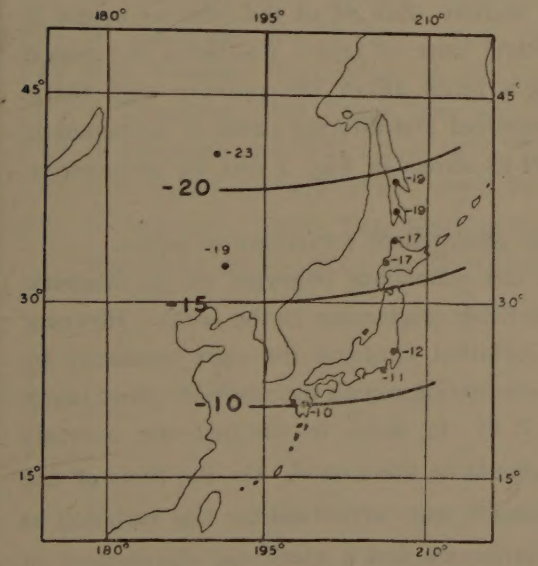

Fig. 10. The distribution of the external part of ΔZ for the same variation. The unit is *gamma*.

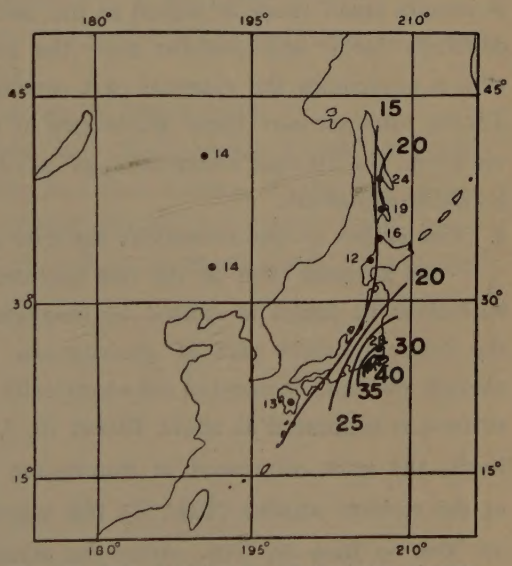

Fig. 11 The distribution of the internal part of ΔZ for the same variation. The unit is *gamma*.

tion of W with that of ΔZ, the external and internal parts of W and ΔZ are calculated for stations in and around Japan by means of E.H. Vestine's method of surface integration [4]. Owing to the irregular distributions of ΔZ, the accuracy of the calculation is not too reliable in general. But as far as the stations in Japan and its neighborhood are concerned, the results should be approximately right because we had

fairly many stations there. Both parts of the potential for the SC are shown respectively in Figs. 6 and 7, while similar results are illustrated in Figs. 8 and 9 for the change at $5h\ 50m$ on June 19. The external and internal parts of ΔZ for the latter are also shown in Figs. 10 and 11. As can be clearly seen in these figures, the distribution of the external origin parts are fairly regular for both variations. On the contrary, the internal origin parts are distributed in a strange way.

Although the anomalous distribution of the internal origin part can be seen less clearly in the case of the SC partly because of the smallness of the amplitude of the variation, we find some characteristic equi-potential lines as well as equal variation lines for ΔZ of internal origin concentrated near the central part of Japan. If we consider that the variations of internal origin are caused by electric currents flowing just under the earth's surface, the currents should flow in the directions which are shown in the figures. It seems quite strange that the induced currents flow to the same direction as that of the inducing currents provided the usual standpoint of electromagnetic induction within a homogeneous earth is adopted. Hence we must imagine some particular conditions beneath Japan.

In Figs. 10 and 11, we can see that the external parts of ΔZ direct upward while those of internal parts direct downward taking almost the same magnitude in the northern part of Japan. This seems to be the reason why the amplitude of ΔZ is usually small there as stated in the last section. But ΔZ of the internal origin is definitely large and positive near the central part of Japan, this being the reason why it overcomes the external part causing a large ΔZ of the positive sign there. Taking into account these tendencies of external and internal parts of geomagnetic variation, the strange distribution of $\Delta Z/\Delta H$ as shown in Fig. 3 can be phenomenologically explained.

4. *The origin of the anomalous behavior of geomagnetic variations in Japan.*

As is made clear in the last section, the anomalous behavior of geomagnetic variations in Japan is caused by magnetic fields originating in the earth. However the internal origin part of geomagnetic variation contains the part produced by electric currents induced in the electrically conducting region the depth of whose upper surface is estimated at about $400km$ [5, 6, 7, 8]. In order to abstract the anomaly itself, the part originated in this region should be eliminated. On the basis of one of the writers' studies (T.R.) [8], this elimination was carried out for the variation at $5h\ 50m$ on June 19, 1936. After the elimination we find a particular distribution of the magnetic field in Japan. This field is well approximated with that of a magnetic dipole situated at a depth of $150km$ under the central part of Japan, the direction of it being approximately north and having a dip of 20°. Though this expression with a dipole is nothing but a conventional model, we must pay attention to the fact that the anomaly is well explained by considering a localized source. We can say nothing, however, why the apparent magnetic dipole occurs on occasions of geomagnetic variations.

5. *Conclusions.*

The writers pointed out an abnormally large ΔZ of short-period geomagnetic variations observed at Hermanus as well as some Japanese observatories. The characteristics in Japan were statistically examined with data from well-distributed observatories. Meanwhile it was made clear that the anomalous behavior in Japan is caused by the magnetic field originated within the earth by analyzing world-wide data from the standpoint of the potential theory. Detailed reports were already published in a series of papers [1] in the Bulletin of the Earthquake Research Institute.

In conclusion, the writers are grateful to Professor M. Hasegawa, Dr. M. Ôta, Professor T. Nagata and Mr. N. Fukushima who are interested in this study and offer useful data to the writers. The writers are also indebted to many geomagneticians in foreign countries who kindly sent copies of megnetograms at the writers' request.

References

[1] T. Rikitake, I. Yokoyama and Y. Hishiyama, Bull. Earthq. Res. Inst., **30**, 207 (1952), **31**, 19 (1953), **31**, 89 (1953), **31**, 101 (1953), **31**, 119 (1953).

[2] S. Chapman and J. Bartels, Geomagnetism Vol. I, 297 (1940).

[3] M. Hasegawa and M. Ôta, Trans. Oslo Meeting, I.A.T.M.E.I.U.G.G., 431 (1950).

[4] E.H. Vestine, Terr. Mag., **46**, 27 (1941).

[5] S. Chapman, Phil. Trans. Roy. Soc. London A, **218**, 1 (1919).

[6] S. Chapman and A.T. Price, Phil. Trans. Roy. Soc. London A, **229**, 427 (1930).

[7] B.N. Lahiri and A.T. Price, Phil. Trans. Roy. Soc. London A, **237**, 509 (1939).

[8] T. Rikitake, Trans. Oslo Meeting I.A.T.M.E.I.U.G.G., 435 (1950). Bull. Earthq. Res. Inst., **28**, 45 (1950), **28**, 219 (1950), **28**, 263 (1950), **29**, 61 (1951), **29**, 539 (1951).

The Thermal Fluctuation After Effect found in the Natural Remanent Magnetic Polarization of Rocks

By Naoto KAWAI and Shōichi KUME
(Geological and Mineralogical Institute, Faculty of Science, Kyoto University)

Abstract

In the study of natural remanent magnetic polarization of rocks, the authors found many kinds of sedimentary rocks whose major part of the polarity may probably be attributed to thermal fructuation after effect resulted under the influence of the geomagnetic field during the geological interval. In this paper are reported the polarity of tertiary rocks observed, and experiments of the related problems carried out in our laboratory.

I. Introduction.

A few years ago, J.W. Graham[1] proposed many ingenious methods for examining the stability of natural remanent magnetic polarization of rock (abbr. N.R.M.). From his numerous field observations it was well confirmed that many rocks kept their initial direction of polarization unchanged through the geological time up to the present. In order to test the said stability of rocks in Japan, the present authors employed one of the Graham's methods. Many pieces of pebbles were sampled from a conglomerate of a known geological age, and their directions were measured by a sensitive astatic magnetometer.[2] Favorable agreements with the Graham's result were obtained in the case of many igneous pebbles. However, the data from sedimentary pebbles obviously showed themselves as the exceptions. Those conglomerates whose pebbles had their direction of the N.R.M. nearly parallel to that of the geomagnetic field have been found from the tertiary basins in Bōsō and Ōsaka. It is quite unlikely that the pebbles in the conglomerate possess such a particular direction in the field, when we assume that the N.R.M. is stable through the geological time. This seemed to suggest the following presumption that the direction of the pebbles might have changed into the present configuration of the polarity from the initial and probably random distribution with which the pebbles had been migrated into the stratum.

After the field examinations, each pebble specimen has carefully been kept in the laboratory in constant orientation since these three years and measuring of the polarization was successively repeated with proper duration of intervals. A distinct change which is exceedingly larger than measuring errors, was observed in both the direction and the intensity of the polarity.

In this paper the data are summarized with an aim of making connection to the Néel's theories[3,4,5] on the thermal fluctuation after effect.

II. Field observations.

The examinations of the stability were carried out at thirteen localities, five sheets of conglomerates being selected from Ōsaka, as well as eight sheets from Bōsō sedimentary basin. About 20 pieces of pebbles were sampled from each conglomerate at each locality and their directions of N.R.M. were measured by the astatic magnetometer. The results are illustrated in Fig. 1A–Fig. 1E. with respect to the following

Fig. 1

typical cases. In these figures the positive magnetic poles of pebbles were adopted and plotted in the Schmidt's equal-areal projection. The solid and hollow circles in the figures represent the poles which are situated respectively on the lower and upper hemi-sphere of the projection and the cross marks correspond to the position of the present geomagnetic field.

The pole distribution of igneous pebbles in a Miocene conglomerate in Ōsaka group is shown in Fig. 1A. (The age of the bed is estimated from palaeontrogical criteria to be older than 10^7 years, whereas the mean intensity of the N.R.M. is 2×10^{-3}C.G.S./cm^3). The poles are distributed in random manner on both the upper and the lower hemi-sphere of the projection with nearly equal population. The result agrees well with the Graham's observation. Meanwhile, the similar examinations were carried out with respect to the sedimentary pebbles in Miocene conglomerate in Bōsō group (The age is nearly of the same order as that of Ōsaka group, but the intensity of the N.R.M., is weaker than the former, ranging from 10^{-4} to 10^{-6}C.G.S./cm^3). Throughout the results of the sedimentary pebbles (Fig. 1B–Fig. 1E), the poles of the polarization are distributed only on the lower hemi-sphere of the projection. As will be seen in Fig. 1D and Fig. 1E, the direction of each pebble is approximately parallel to the present geomagnetic field vector. In contrast to the diverging distribution of the poles on the projection of Fig. 1A, the directions of these pebbles remarkably converge to the cross mark on the diagrams.

III. The change of polarization in the laboratory.

The pebble specimens which had been prepared for the stability test were preserved in the laboratory since these three years. Each of the pebble specimens was carefully kept with the fixed orientation so that the earth's magnetic field might

apply in the direction appropriately deviated from that of the polarity. And the direction was measured successively, allowing the interval duration of 2, 16, 43, 110, 380, 785 and 1000 days respectively. In almost every sedimentary specimen except in the case of the pebble A, changes of the polarization were sufficiently detectable by our measuring equipment. The angular change of the polarization is illustrated by the pole movement in Fig. 2–3, where the durations of time (in days) are shown by the number suffixed to the poles. The following tendencies may be to be noticed.

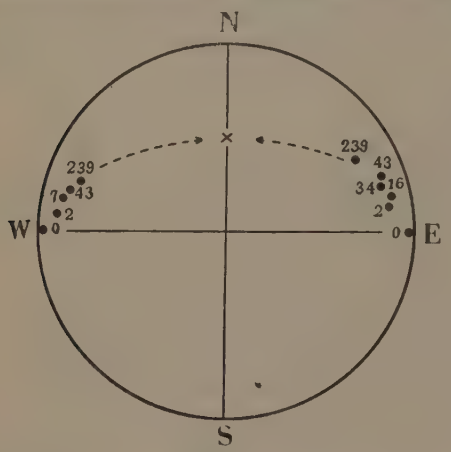

Fig. 2

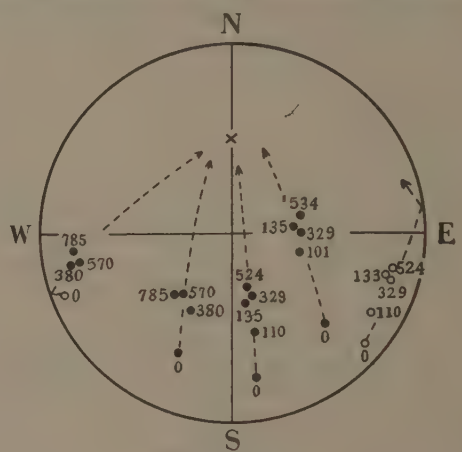

Fig. 3

×: Position of present geomagnetic field ○: Positive magnetic pole on upper hemi-sphere ●: Positive magnetic pole on lower hemi-sphere

(1) During the change the direction of the polarization is generally restricted on a definite plane which is determined by the two direction, one being the same as the initial direction of the polarity before the change, and other that of the geomagnetic field in laboratory.

(2) The velocity of the pole movement was greater at the beginning of the change, and then has decreased gradually to the present. Within our experimental time interval ranging from 2 to 1000 days so far, the angular changes are approximately proportional to log t. Amount of the angular change vs. log t curves are shown in Figs. 4A–4E. The letters A, B, C, D, E in these figures correspond to the curves obtained from the pebbles A, B, C, D and E respectively.

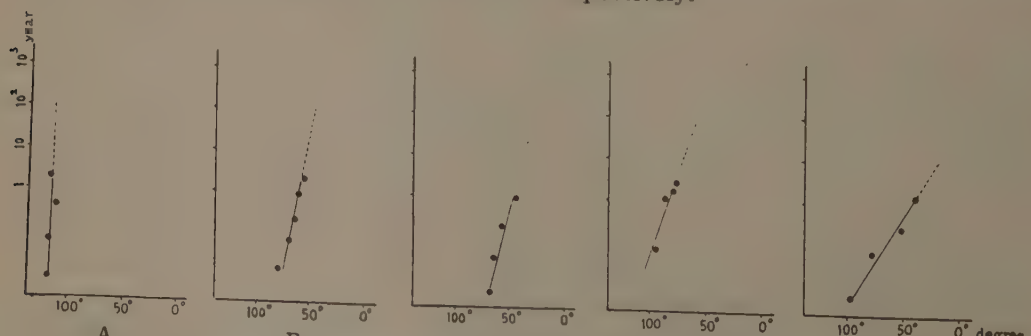

← Deviation from the Direction of the Present Geomagnetic Field

Fig. 4

(3) Although the slopes of the curves take various values with respect to rock facies, there may be a qualitative but close correlation: the pebbles with better convergence in the conglomerate (in situ) have faster rate of change in the laboratory. Comparison of Fig. 1 to Fig. 4 demonstrates this correlation.

IV. Temperature dependence of the change of polarization.

Another trial to observe the change of the polarization was carefully examined, keeping the temperature of the specimens appropriately constant throughout the experimental time interval. One of the pebble specimens was kept in a constant orientation so that the geomagnetic field may be applied in the direction perpendicular to that of the specimen polarity. And the polarity was measured by the astatic magnetometer. The change of the polarity in both its direction and intensity is illustrated by the vectorial representation of the polarity during the experiment (Fig. 5). Meanwhile, the pebble specimens were ground into powder or were freely released into grain with least mechanical shock as possible.

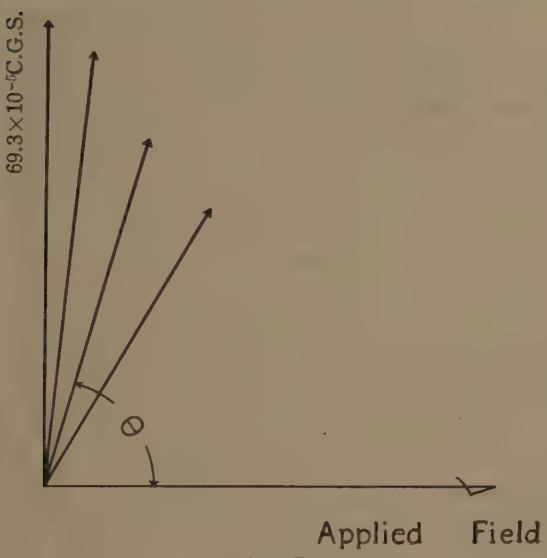

Fig. 5

The powder was sealed in a glass cylinder so that each grain may cancel their polarization with other, and the test specimens with non-permanent polarization were prepared. The specimens were kept during 200 hours at a constant temperature in a thermostat under the application of a constant magnetic field. By these treatments the sufficiently measurable polarizations were induced in the specimens. And by measuring the intensity with proper duration of intervals it was found that the intensity increased with time in a manner as is illustrated in Fig. 6. Similar examinations were carried out with various constant temperatures, 28°C, 40°C, 55°C and 68°C. The results obtained at each experiment are shown respectively in Fig. 7.

From the experiments it may be noticed that the intensity of polarization induced by the experimental procedure is nearly of the same order as that of the N.R.M. which we could originally find in the field, although the ratios of the former to the latter take various values in different specimen

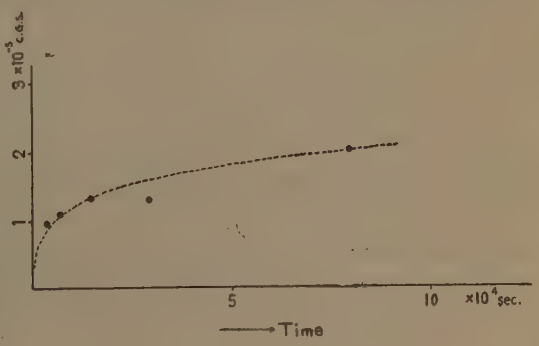

Fig. 6

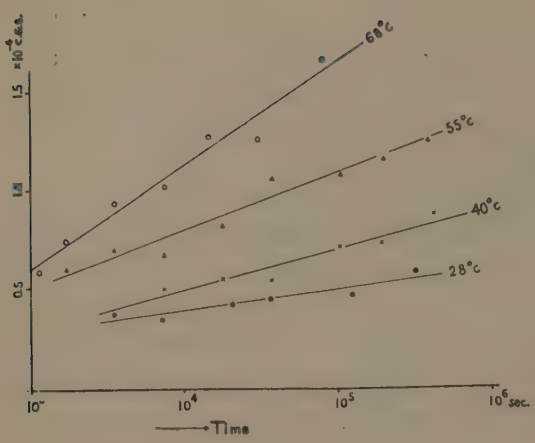

Fig. 7

pieces.

The direct correlation of our results to the Néel's theories on the thermal fluctuation after effect[3,4,5] and the related experiments by many authorities[6,7,8,9] seems to be difficult in the present stage. The problem will be postponed until the future when the sufficient data of our experiments will have been accumulated.

V. Acknowledgements.

The author's hearty acknowledgments are first due to Prof. Emeritus M. Matsuyama, Prof. H. Hasegawa, Prof. N. Kumagai, Prof. H. Takagi who encouraged us with valuable guidances. Their cordial thanks are also due to Prof. T. Nagata of Tokyo University and N. Ikebe of Ōsaka Municipal University for their kind advices and many suggestions throughout the whole study.

References

(1) J.W. Graham, Journ. Geophys. Res, **54**, 131 (1949)
(2) N. Kawai, Journ. Geophys. Res. **56**, 73 (1951)
(3) L. Néel, Ann. Géophys. **4**, 99, (1949)
(4) L. Néel, J. Physique. Rad. **11**, 49 (1950)
(5) L. Néel, J. Physique. Rad. **12**, 339 (1951)
(6) J.C. Barbier, J. Physique. Rad. **12**, 352 (1951)
(7) R. Street & J.C. Woolley, Proc. Phys. Soc., A. **92**, 562 (1949)
(8) T. Nagata, Bull. Earthquake Res. Insti. **21**, 1 (1943)
(9) E.Thellier & O. Thellier, Ann. Geophys. **1**, 37 (1944)

On Distribution of Nitrogen in the Upper Atmosphere*

By Teruo SATO
(Geophysical Institute, Kyoto University)

Abstract

In this paper the dissociation of the nitrogen in the upper atmosphere is studied. It is considered that the nitrogen atom is produced by dissociative recombination of the positive nitrogen ion and the electron, and by the pre-dissociation by the absorption in the Lyman-Birge-Hopfield band. The former is effective in the region above about 120km, while the latter predominent below that level. The disappearance of the nitrogen atom is mainly due to the recombination by two or three body collision. Approximately, the fomer mechanism of disappearance seems to be preponderant over the latter in the region where the dissociative recombination is conspicuous. Hence, two pairs of equations in an equilibrium state are solved. In the calculations, it is assumed that the temperature is constant throughout the region; the ratio of the concentation of the oxygen atom to that of the sum of the nitrogen is one-half; and the distribution of total nitrogen follows the law of gas in a static equilibrium, though the distribution of nitrogen molecule with height is not given previously. The results show that the nitrogen begins to dissociate at the level from 120km to 130km, and proceeds to completion at about 160km–220km. The concentration of the nitrogen atom has peak at about 140km–150km altitude and its magnitude is of the order of 10^{10}/c.c..

§ 1. Introduction

Although the dissociation of the oxygen has been studied by many workers (for example, Rakshit [1], Penndorf [2] and Moses and Ta-You Wu [3]), the dissociation of the nitrogen has not been researched in detail. This problem is very important because the formation theory of the ionized region, especially, of that above the E region has a close relation to the kind and distribution of the absorbing particle of the solar radiation. Since the measurement of the pressure and that of the density in the upper atmosphere by the rocket flight have been made, it becomes necessary to know dissociations of the oxygen and the nitrogen for deducation of the concentration of the particle and the temperature in any height. The Rocket Panel [4], for example, assumes that the oxygen and the nitrogen begin to dissociate at the levels of 80km and 120km, and proceed to completion at 120km and 220km respectively. There are

* Contribution to Geophysical Papers dedicated to Prof. M. Hasegawa on his sixtieth birthday.

two main mechanisms of the dissociation of the nitrogen. One is the dissociation suggested by Bates and Massey [5], Bates [6], and Mitra [7], in which the nitrogen molecule is ionized by radiation with a wave length below 795 Å, the positive nitrogen ion produced combines with an electron, and it dissociates into two nitrogen atoms. The other is the pre-dissociation suggested by G. Herzberg and L. Herzberg [8], in which the nitrogen molecule is excited by radiation with the wave length 1150 Å–1250 Å and later this excited molecule dissociates into two atoms. The former suggestion is useful in the upper inoized region. Recentely Bates [6] and Deb [9] calculated the distribution of the nitrogen atom using these two mechanisms. Bates computes mainly the distribution of nitrogen atom at the level of the E region, including the disappearance of the nitrongen atom due to the existence of the oxygen atom and the nitric oxide. According to Deb, the dissociation of nitrogen does not exceed fifty percent even at the level of 400 km. In his study, however, the distribution of the nitrogen molecule with height in an equilibrum state is assumed, which in computation must be treated as unknown. Hence it appears that the results are unsatisfactory. In our study the two mechanisms of dissociation are still adopted, and for the disappearance of the atom the recombination by two or three body collisions are used corresponding to the two dissociation mechanisms, as mentioned in Appendix I. The distribution of the nitrogen molecule with height is not given, but it is assumed that the sum of the total nitrogen particles distributes in such a way as a gas in static equilibrium. The ratio of the concentration of the total nitrogen to that of the oxygen atom is taken to be 2.

§ 2. Production and Disappearance of Nitrogen Atom

(i) Production of Nitrogen Atom

Bates and Massey, and Mitra suggested that in the F region the following ionization and dissociative recombination are effective,

$$\left.\begin{aligned} &N_2+h\nu\rightarrow N_2^{+}+e, \quad \text{(a)} \\ &N_2^{+}+e\rightarrow 2N. \quad \text{(b)} \end{aligned}\right\} \qquad (1)$$

The energy which ionizes the nitrogen molecule is that above 15.6 eV (795 Å). On the other hand, G. Herzberg and L. Herzberg suggested that the nitrogen is also dissociated by pre-dissociation by the radiation in a range 1150 Å–1250 Å as follows,

$$\left.\begin{aligned} &N_2(X^1\Sigma_g^{+})+h\nu \rightarrow N_2(a^1\Pi_g), \quad \text{(a)} \\ &N_2(a^1\Pi_g) \rightarrow 2N. \quad \text{(b)} \end{aligned}\right\} \qquad (2)$$

According to Bates, this process is effective in the lower region than the F region. Hence in the computation, (1) or (2) may be neglected corresponding to the height concerned. Bates also pointed out that the nitrogen atom is produced by dissociation of NO as follows,

$$\left.\begin{aligned} &NO(X^2\Pi)+h\nu(6.5eV) \rightarrow NO(A^2\Sigma^{+} \text{ or } C^2\Sigma^{+}), \\ &NO(A^2\Sigma^{+} \text{ or } C^2\Sigma^{+}) \rightarrow N+O. \end{aligned}\right\} \qquad (3)$$

This appears to be effective in the same region as that in which the process (2) is preponderant. According to Bates, when (3) and (6), (7) in § 2 (ii) are taken into account, the concentration of the nitrogen atom becomes smaller than that in the pure nitrogen atmosphere. But even for the latter, the concentration is very small compared with the total particle. As we are interested mainly in the upper region above the E region, and the computation is complicated we do not take into account these reactions. Hence, the results in the lower atmosphere will show the upper limit of the concentration of the nitrogen atom. According to Appendix I (a), the range in which the process (1) is usable, is above the region where the concentration of the total particle is at least 10^{12}/c.c., and process (2) is usable below that level.

(ii) Disappearance of Nitrogen Atom

Moses and Ta-You Wu and Deb showed that oxygen and nitrogen atom disappears by recombination by two-body collision rather than three-body collision, except in the very low atmosphere. This reaction for nitrogen atom is given by

$$N+N \rightarrow N_2+h\nu. \qquad (4)$$

But Bates, Penndorf and Mitra showed that the rate constant by three-body collision is larger than that by two-body collision, and is of the order of 10^{-32}cm^6/s. Two ways of three-body collision are given by

$$N+N+M \rightarrow N_2+M, \qquad (5)$$

$$N+O+M \rightarrow NO+M, \qquad (6)$$

where M is a third body which takes away the excess of the energy and momentum.

Another process is given by Bates as follows,

$$N+NO \rightarrow N_2+O. \qquad (7)$$

We neglect (6) and (7) for the reason mentioned above in (i). In Appendix I (b) it is shown that the process (4) is predominent above the level which has the concentration of the total particle of at least 10^{11}/c.c.. Thus the process (1) and (4) are considered to be active in the same range of height and (2) and (5) in another range of height.

§ 3. Absorption of Solar Radiation

(i) The solar energy in a spectral range below 795 Å is not only absorbed by the nitrogen molecule, but also absorbed by the oxygen atom and the nitrogen atom. The oxygen atom is ionized by the radiation with the energy above 13.6 eV (910 Å) and the nitrogen atom by the radiation above 14.5 eV (850 Å). According to Bates and Seaton [10], the absorption coefficient is 2.6×10^{-18}cm^2 for the oxygen atom and 9×10^{-18}cm^2 for the nitrogen atom. Nicolet [11] pointed out that the absorption coefficient for the oxygen atom is 4.5×10^{-18}cm^2 for the radiation between 13.6 eV and 17 eV, 1.1×10^{-17}cm^2 between 17 eV and 18.6 eV and 1.6×10^{-17}cm^2 above 18.6 eV, and 2×10^{-17}cm^2 for the nitrogen atom. These values are comparable with the absorption coefficient of the nitrogen molecule given by Bates and Massey which is about 1×10^{-17}cm^2. Thus the

radiation decreases more rapidly in the case of the absorption by sum of these different kinds of particles than the case of the absorption only by nitrogen molecules.

The concentration of ionized nitrogen molecule produced by the process (1) is given by

$$q_1 = A_{N_2} S_{1\infty} \exp[-\int_h^\infty \{A_{N_2}[N_2] + A_N[N] + A_0[O]\} \sec\chi \, dh][N_2], \tag{8}$$

where brackets represent the concentration of the particle per c.c., A_r the absorption coefficient referred to the particle r, which is considered to be independent of the wave-length of the radiation, $S_{1\infty}$ the number of mean total quanta available, h the coordinate of height and χ the zenith angle. If we take $A_{N_2} \simeq A_0 \simeq A_N = 10^{-17}\text{cm}^2$, and assuming

$$[O] = 1/2\{[N_2] + [N]\}, \tag{9}$$

then (8) becomes

$$q_1 = A_{N_2} S_{1\infty} \exp[-1.5 A_{N_2} \int_h^\infty \{[N_2] + [N]\} \sec\chi \, dh][N_2]. \tag{10}$$

(ii) The concentration of nitrogen atom produced by pre-dissociation process is given by

$$q_2 = B_{N_2} g_N S_{2\infty} \exp[-\int_h^\infty B_{N_2}[N_2] \sec\chi \, dh][N_2], \tag{11}$$

where $S_{2\infty}$ represents the number of mean total quanta available, B_{N_2} the absorption coefficient which is independent of the wave length of the radiation, and g_N the rate constant of the transition in (2) (b).

§ 4. Formulae for the Equilibrium State

Case I. Region in which the processes (1) and (4) are effective.

The variations of $[N_2^+]$ and $[N]$ with the time are given by

$$\frac{d[N_2^+]}{dt} = q_1 - \alpha[N_2^+][e], \tag{12}$$

$$\frac{[dN]}{dt} = \alpha[N_2^+][e] - \kappa_1[N]^2, \tag{13}$$

where $[e]$ represents the density of the electron per c.c., and κ_1, α the rate constants of two body collision and dissociative recombination respectively. In an equilibrium state we have

$$q_1 = \kappa_1[N]^2,$$

i.e.,

$$A_{N_2} S_{1\infty} \exp[-1.5 A_{N_2} \int_h^\infty \{[N_2] + [N]\} \sec\chi \, dh][N_2] = \kappa_1[N]^2. \tag{14}$$

Case II. Region in which processes (2) and (5) are effective.

A variation of $[N_2]$ is given by

$$\frac{d[N_2]}{dt} = -q_2 + \kappa_2[N]^2[M], \tag{15}$$

where κ_2 is the rate constant of three-body collision. In an equilibrium state it becomes

$$q_2=\kappa_2[N]^2[M]$$

i.e.,

$$B_{N_2}g_N S_{2\infty}\exp[-\int_h^\infty B_{N_2}[N_2]\sec\chi\, dh][N_2]=\kappa_2[N]^2[M]. \tag{16}$$

§ 5. Calculations of Dissociation of Nitrogen

Case I.

we start to solve the equation (14).

(14) becomes

$$\exp[-1.5A_{N_2}\int_h^\infty\{[N_2]+[N]\}\sec\chi\, dh]=\frac{\kappa_1[N]^2}{A_{N_2}S_{1\infty}}. \tag{17}$$

We assume that

$$dp=-\{2[N_2]+[N]\}m_N g\,dh, \tag{18}$$

$$p=\{[N_2]+[N]\}kT, \tag{19}$$

where p represents partial pressure, m_N an atomic mass of the nitrogen, g and k gravitational constant and Boltzmann's constant respectively, and T the temperature. Then

$$\frac{d}{dh}\Big[\{[N_2]+[N]\}kT\Big]=-\{2[N_2]+[N]\}m_N g. \tag{20}$$

If we take T as constant (20) becomes as follows,

$$\frac{d}{dh}\{[N_2]+[N]\}=-\{2[N_2]+[N]\}\frac{m_N g}{kT}=-2\{[N_2]+[N]\}\frac{1}{H_N},\quad H_N=\frac{kT}{m_N g}. \tag{21}$$

When we put

$$[N_2]+[N]\equiv Q, \tag{22}$$

we obtain from (21)

$$\frac{d}{dh}Q=-[Q+[N_2]]\frac{1}{H_N}.$$

Hence, after integration we get

$$Q=\frac{1}{H_N}\Big\{\int_h^\infty Q dh+\int_h^\infty[N_2]\Big\}dh, \tag{23}$$

where Q_∞ which represents the value of Q in the infinity is neglected compared with Q.

From (23) we get

$$-\int_h^\infty Q dh=-QH_N+\int_h^\infty[N_2]dh. \tag{24}$$

(i) Region of Small Dissociation

In this region we have following approximate expressions

$$Q\simeq[N_2], \tag{25}$$

$$\int_h^\infty Q\,dh=\int_h^\infty[N_2]\,dh+\int_h^\infty[N]dh\simeq\int_h^\infty[N_2]\,dh. \tag{26}$$

The limit of the dissociation that the approximation (26) holds is examined in Appendix II (a). Thus

$$-\int_h^\infty Q\,dh=\frac{-1}{2}QH_N\simeq-\frac{1}{2}[N_2]H_N. \tag{27}$$

(17) becomes using (22), (24) and (27) as follows,

$$\exp\{-0.75 A_{N_2} H_N [N_2]\} = \frac{\kappa_1 [N]^2}{A_{N_2} S_{1\infty} [N_2]}, \quad \text{for} \quad \sec\chi = 1. \tag{28}$$

(ii) Region of Large Dissociation

In this region following approximations hold.

$$Q \simeq [N], \tag{29}$$

$$\int_{\infty}^{h} [N_2]\, dh \ll Q H_N. \tag{30}$$

The limit of the dissociation that the approximation (30) holds is examined in Appendix II (b). From (24) we get

$$-\int_h^{\infty} Q\, dh = -QH_N \simeq -[N] H_N. \tag{31}$$

Then (17) becomes as follows,

$$\exp\{-1.5 A_{N_2} H_N [N]\} = \frac{\kappa_1 [N]^2}{A_{N_2} S_{1\infty} [N_2]}, \quad \text{for} \quad \sec\chi = 1. \tag{32}$$

If $[N]/[N_2]$ is estimated, the values of $[N_2]$ or $[N]$ which satisfies (28) or (32) are obtained. But in this method it is unable to compute the values of $[N_2]$ and $[N]$ in the dissociation from about 20 percent to 50 percent. In the calculations of (28) and (32), $S_{1\infty}$ is taken to be $2\times10^9/\mathrm{cm}^2/\mathrm{s}$ by interpolation of the curve given by Nicolet [12]; κ_1 is taken to be $10^{-18}\mathrm{cm}^3/\mathrm{s}$, $10^{-19}\mathrm{cm}^3/\mathrm{s}$ and $10^{-20}\mathrm{cm}^3/\mathrm{s}$ as mentioned in Appendix I, and as the value of H_N 2×10^6cm, 3×10^6cm and 5×10^6cm are used. In the case that (28) and (32) cannot be used, the following method is used. That is, when $[N_2]$ and $[N]$ are known for the upper and lower limits of the dissociation we can know immediately the values of Q and $\int_h^{\infty} Q\, dh$ by (25), (27) and (29), (31).

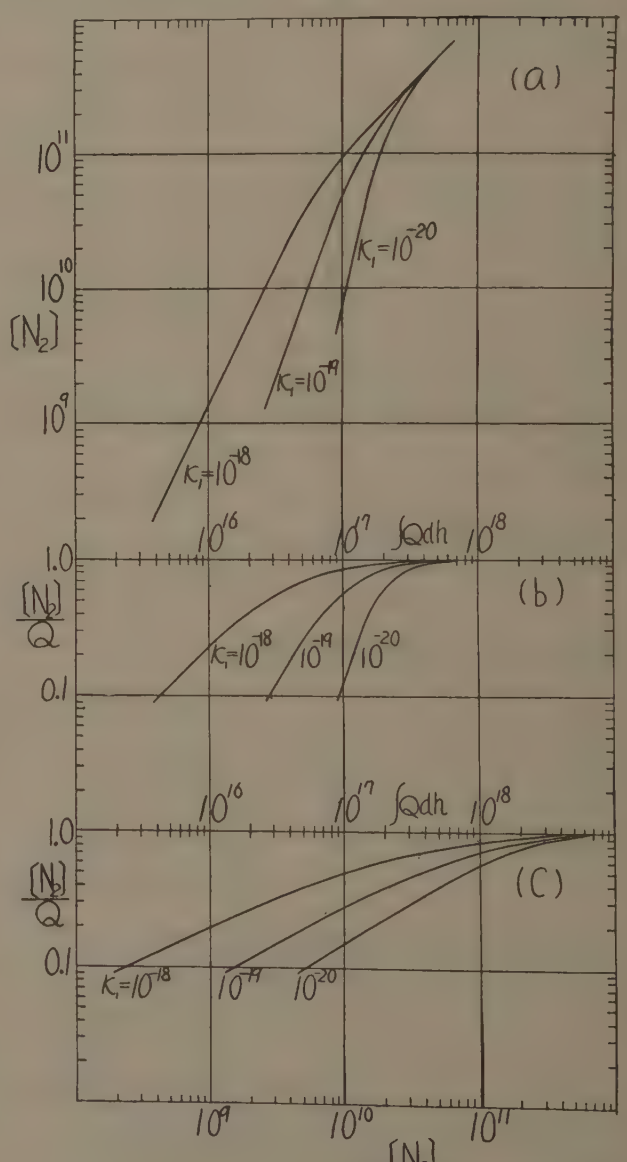

Fig. 1 Curves of $[N_2]$ *vs.* $\int Q dh$, $[N_2]/Q$ *vs.* $\int Q dh$ and $[N_2]/Q$ *vs.* $[N_2]$ for $\kappa_1 = 10^{-18}\mathrm{cm}^3/\mathrm{s}$, $10^{-19}\mathrm{cm}^3/\mathrm{s}$ and $10^{-20}\mathrm{cm}^3/\mathrm{s}$ when $H_N = 2\times10^6$cm.

Accordingly we are able to plot the curve $[N_2]/Q$ *vs.* $[N_2]$, $[N_2]/Q$ *vs.* $\int_h^\infty Q dh$, or $[N_2]$ *vs.* $\int_h^\infty Q dh$. By the interpolation of these curves we can easily obtain the values of $[N_2]$, Q and $\int_h^\infty Q dh$ for various degrees of dissociation. In Fig. 1 (a), (b) and (c), curves mentioned above for $H_N = 2\times10^6$cm are shown.

After knowing the value of Q it is easily able to get the partial pressure. That is,

$$p = QkT. \tag{33}$$

The values of $[N_2]/Q$, $[N]$, $[N_2]$, Q, $\int_h^\infty Q dh$ and p are shown in Table I for $H_N = 2\times10^6$cm

Table I

$\frac{[N_2]}{Q}$	$\int_h^\infty Q\,dh$ (/cm² column)		$[N_2]$ (/c.c.)		Q (/c.c.)		$[N]$ (/c.c.)		p (dyne/cm²)	
	$\varkappa_1=10^{-18}$	$\varkappa_1=10^{-19}$	$\varkappa_1=10^{-18}$	$\varkappa_1=10^{-19}$	$\varkappa_1=10^{-18}$	$\varkappa_1=10^{-19}$	$\varkappa_1=10^{-18}$	$\varkappa_1=10^{-19}$	$\varkappa_1=10^{-18}$	$\varkappa_1=10^{-19}$
1.0	4.15×10^{17}	5.42×10^{-17}	4.15×10^{11}	5.42×10^{11}	4.15×10^{11}	5.42×10^{11}	0	0	1.99×10^{-2}	2.48×10^{-2}
0.9	1.55×10^{17}	2.55×10^{-17}	1.55×10^{11}	2.55×10^{11}	1.72×10^{11}	2.83×10^{11}	1.72×10^{10}	2.83×10^{10}	7.88×10^{-3}	1.32×10^{-2}
0.8	7.82×10^{16}	1.73×10^{-17}	7.30×10^{10}	1.61×10^{11}	9.12×10^{10}	2.01×10^{11}	1.82×10^{10}	4.02×10^{10}	4.17×10^{-3}	9.13×10^{-3}
0.7	5.46×10^{16}	1.34×10^{-17}	4.60×10^{10}	1.01×10^{11}	6.55×10^{10}	1.43×10^{11}	1.95×10^{10}	4.30×10^{10}	3.06×10^{-3}	6.56×10^{-3}
0.6	3.73×10^{16}	1.12×10^{-17}	2.75×10^{10}	7.00×10^{10}	4.66×10^{10}	1.16×10^{11}	1.86×10^{10}	4.64×10^{10}	2.11×10^{-3}	5.10×10^{-3}
0.5	2.62×10^{16}	9.07×10^{-16}	1.55×10^{10}	4.30×10^{10}	3.10×10^{10}	8.60×10^{10}	1.55×10^{10}	4.30×10^{10}	1.42×10^{-3}	3.96×10^{-3}
0.4	1.95×10^{16}	7.23×10^{-16}	7.00×10^{9}	2.35×10^{10}	1.75×10^{10}	5.90×10^{10}	1.05×10^{10}	3.54×10^{10}	8.12×10^{-4}	2.71×10^{-3}
0.3	1.33×10^{16}	5.74×10^{-16}	3.10×10^{9}	1.35×10^{10}	1.03×10^{10}	4.50×10^{10}	7.21×10^{9}	3.10×10^{10}	4.74×10^{-4}	2.06×10^{-3}
0.2	8.55×10^{15}	4.30×10^{-16}	1.05×10^{9}	5.50×10^{9}	5.31×10^{9}	2.75×10^{10}	4.25×10^{9}	2.20×10^{10}	2.41×10^{-4}	1.26×10^{-3}
0.1	4.31×10^{15}	2.80×10^{-16}	2.40×10^{8}	1.60×10^{9}	2.40×10^{9}	1.60×10^{10}	2.16×10^{9}	1.54×10^{10}	1.12×10^{-4}	7.33×10^{-4}

In this method we are unable to know the degree of dissociation at a certain height because the distribution $[N_2]$ or Q are not given, except the expressions (18) and (19). This difficulty is excluded using the data of measurement of the rocket flight in which the pressure and density are directly obtained. When we use (9), the observed pressure is given by

$$p_{obs} = 1.5p = 1.5QkT. \tag{34}$$

Using (34) we get the distribution of the nitrogen atom and molecule with height. Fig. 2 (a), (b) and (c) show these curves for $H = 2\times10^6$cm, 3×10^6cm and 5×10^6cm respectively. The full lines show the distribution of $[N]$ and the dotted lines show the distribution of $[N_2]$ (only for (c)). It is found that Q and maximum $[N]$ for smaller H_N are greater than those for greater H_N. The curves of the distribution of $[N]$ are alike one another and have maximum value at about 140km–150km altitudes, and dissociations begin at about 130km and proceed to completion at about 150km–160km, 160km–180km and 200km–220km corresponding to $\kappa_1 = 10^{-20}$cm³/s 10^{-19}cm³/s and 10^{-18}cm³/s respectively. To determine an appropriate value of H_N, the

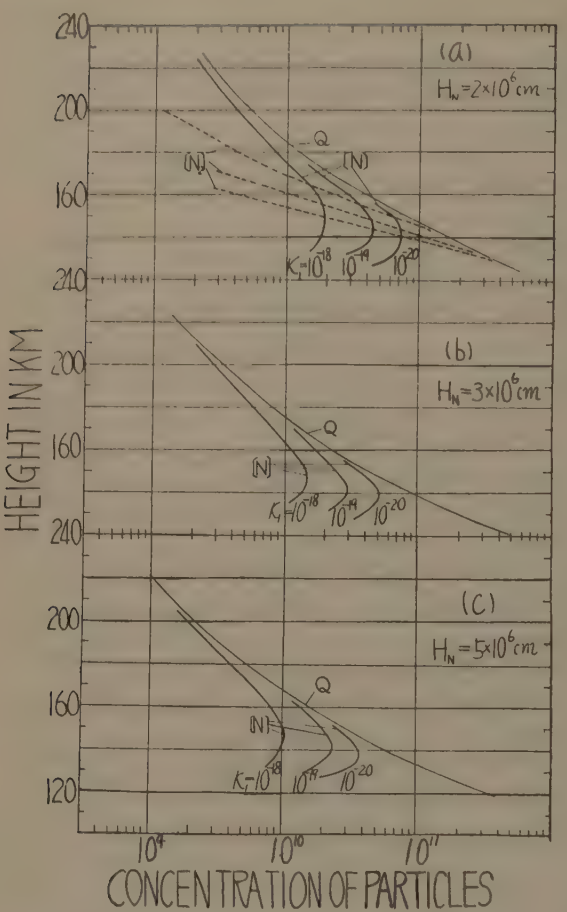

Fig. 2 Curves of distributions of Q (hair lines), $[N]$ (full lines) and $[N_2]$ (dotted lines, only for (a)) with height for $\varkappa_1=10^{-18}$cm³/s, 10^{-19}cm³/s and 10^{-20}cm³/s when $H_N=2\times10^6$ cm (a), 3×10^6cm (b) and 5×10^6cm.

following method is used. As is shown in Fig. 2, above 200km it appears that $[N]\gg[N_2]$. Then in that region the following relations are obtained.

$$p_{obs}=\{[N]+[O]\}kT=3[O]kT, \quad (35)$$

$$d_{obs}=[N]m_N+[O]m_o, \quad (36)$$

where m_0 is the atomic mass of the oxygen and d_{obs} is the observed density. Thus

$$T=[2m_N+m_0]p_{obs}/3kd_{obs}$$
$$=1.86\times10^{-7}\frac{p_{obs}}{d_{obs}}, \quad (37)$$

$$[N]=\frac{2p_{obs}}{3kT}. \quad (38)$$

For the region from 190km to 220km T and N are shown in Table II.

Table II

h (km)	T (°K)	$[N]$ (/c.c.)
220	463	1.92×10^9
210	436	2.96×10^9
200	406	4.66×10^9
190	372	7.20×10^9

Now it is necessary that the value of $[N]$ deduced in the calculation is consistent approximately with that in Table II. Hence it appears to be better to take it as $H_N=2\times10^6$cm. In conclusion, the distribution of $[N]$ is given in Fig. 2 (a) and the maximum of $[N]$ is of the order of 10^{10}/c.c..

Case II.

In the case of the equation (16) the expressions (18) and (19) are also used. From (23) we obtain

$$\int_h^\infty[N_2]=H_NQ-\int_h^\infty Q\,dh, \quad (39)$$

and approximately $[M]=3Q/2$. When $[N_2]\gg[N]$

$$\int_h^\infty[N_2]dh\simeq H_NQ-\int_h^\infty[N_2]dh.$$

Hence

$$\int_h^\infty[N_2]\simeq\frac{1}{2}H_NQ\simeq\frac{1}{2}H_N[N_2]. \quad (40)$$

Substituting (40) in (16), we get

$$\exp\left\{-B_{N_2}\frac{1}{2}H_N[N_2]\right\}=\frac{1.5\kappa_2[N]^2[N_2]}{B_{N_2}g_N S_1}. \tag{41}$$

When we give $[N]/[N_2]$, $[N_2]$ which satisfies (41) is obtained. Rate constants B_{N_2}, g_N are taken to be 10^{-20}cm^2, 10^{-5}/s derived by Deb in one case and $B_{N_2}g_N S_{2\infty}=10^{-12}$ derived by Bates is used in another case. κ_2 is taken to be 1.5×10^{-32}(c.c.)^2/s computed by Bates. $S_{2\infty}$ is taken to be 3×10^{10}/cm^2/s from the curve derived by Nicolet. The results obtained using these values are shown in Table III and in Fig. 3. It is found that the value of $[N]$ is almost the same magnitude through the levels from 130km to 90km and very small compared with the value of Q.

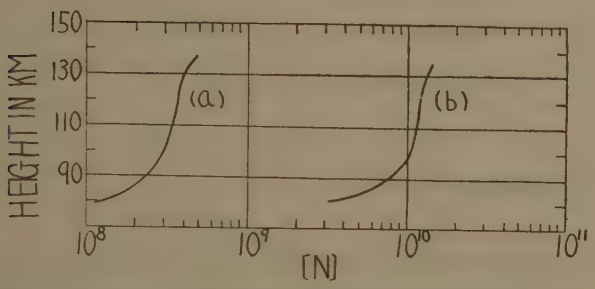

Fig. 3 Curves of distribution of N with height in the lower atmosphere for $B_{N_2}g_N S_{2\infty}=3\times10^{-15}$ (a) and $B_{N_2}g_N S_{2\infty}=10^{-12}$ (b).

Table III

h	$[N]$		Q
	$B_{N_2}g_N S_{2\infty}=10^{-12}$	$B_{N_2}g_N S_{2\infty}=3\times10^{-15}$	
130(km)	1.3×10^{10}(/c.c.)	4.0×10^{9}(/c.c.)	3.3×10^{11}(/c.c.)
120	1.2×10^{10}	3.6×10^{9}	7.6×10^{11}
110	1.1×10^{10}	3.4×10^{9}	2.5×10^{12}
100	1.0×10^{10}	2.8×10^{9}	1.1×10^{13}
90	7.8×10^{9}	2.5×10^{8}	6.0×10^{13}
80	2.5×10^{9}	1.2×10^{8}	4.0×10^{14}

§ 6. Discussions

The results obtained in our method show that the dissociation of the nitrogen begins at the level of 120km–130km and proceeds to completion at the level from 180km to 220km corresponding to the various values of rate constants used here. This is well consistent with the assumption of the dissociation by the Rocket Panel and Callmann [13]. The height of the beginning of the dissociation varies slightly for the conspicuous variation of the rate constant, while the height of completion of the dissociation varies greatly. Hence many constants used here must be studied in detail. Further the assumptions (18), (19) and (9) in the calculation should be minutely examined, though it is unlikely that the results vary remarkably. Thus the nitrogen above the level of about 200km appears to be almost in the atomic state, but this result is not yet conclusive. Bates [14] recently asserts, based on the spectroscopic experiment of the auroral spectrum, that the contribution of the molecular particle to the ionization in the $F2$ region is unimportant. Judging from our results that may

hold. As the dissociation of the nitrogen may remarkably influence on the formation theory of the $F1$ and $F2$ regions, it hopes that more accurate computations are made.

Acknowledgements

The author wishes to express his thanks to Prof. M. Hasegawa for his kind advice, and Prof. K. Maeda for giving valuable guidance and help in the course of this study.

Appendix I

(a) The Range of Application of Dissociative Recombination and Pre-dissoeiation

The effectiveness of the two dissociation processes is known by comparing q_1 and q_2. From (10) and (11), q_1 and q_2 are written again for $\cos\chi=1$,

$$q_1=S_{1\infty}A_{N_2}\exp\left[-1.5\,A_{N_2}\int_h^\infty Q\,dh\right][N_2],$$

$$q_2=S_{2\infty}B_{N_2}g\exp\left[-B_{N_2}\int_h^\infty [N_2]\,dh\right][N_2].$$

In these expressions A_{N_2}, B_{N_2}, g_N, $S_{1\infty}$, $S_{2\infty}$ are given as follows,

	$A_{N_2}=10^{-17}\mathrm{cm}^2$	Bates and Massey,
	$B_{N_2}=10^{-20}\mathrm{cm}^2$	Deb,
	$g_N=10^{-5}/\mathrm{s}$	Deb,
	$S_{1\infty}=2\times10^{9}/\mathrm{cm}^2/\mathrm{s}$ $S_{2\infty}=3\times10^{10}/\mathrm{cm}^2/\mathrm{s}$	Nicolet,
or	$B_{N_2}g_NS_{2\infty}=10^{-12}$	Bates.

At first, we adopt values given by Deb for B_{N_2}, g_N, then

$$\frac{q_1}{q_2}=10^{7}\exp\left[-1.5\times10^{-17}\int_h^\infty Q\,dh\right]. \tag{42}$$

$$\frac{q_1}{q_2}=1 \quad \text{when} \quad 1.5\times10^{-17}\int_h^\infty Q\,dh\simeq16.$$

Hence, $$\int_h^\infty Q\,dh=\frac{16}{1.5\times10^{-17}}\simeq10^{18}.$$

In Table I this is the value corresponding to the level $[N_2]\gg[N]$.

Thus $$H_N[N_2]=2\int_h^\infty Q\,dh=2\times10^{18},$$

$$[N_2]=\frac{2\times10^{18}}{2\times10^{6}}=10^{12}.$$

When we use $g_NB_{N_2}S_{2\infty}=10^{-12}$ given by Bates,

$$\frac{q_1}{q_2}=3\times10^{4}\exp\left[-1.5\times10^{-17}\int_h^\infty Q\,dh\right], \tag{43}$$

$$\frac{q_1}{q_2}=1 \quad \text{when} \quad 1.5\times10^{-17}\int_h^\infty Q\,dh=8.5.$$

Hence $$[N_2]=\frac{5.6\times10^{17}}{10^{6}}=5.6\times10^{11},$$

Consequently the dissociative recombination is more effective above the level where the total perticle is at least 5.6×10^{11}/c.c..

(b) Comparison between Two-body Collision and Three-dody Collision

The ratio of the recombination by three-body collision to that by two-body collision is given by

$$r=\frac{(1-\theta)n\kappa_2}{\kappa_1} \tag{44}$$

where n is the concentration of the total of the different kinds of particles, θ is the ratio of the concentration of recombinig particle to n. κ_1 and κ_2 are given by several authors as follows,

$\kappa_1=10^{-16}$(cm³/s) Herzberg [15], for oxygen atom,
$10^{-18}-10^{-19}$ Deb, for nitrogen atom produced by dissociative recombination,
10^{-21} Deb, for nitrogen atom produced by pre-dissociation,
10^{-20} Nicolet [16], for oxygen atom,
and $\kappa_2=10^{-30}$(cm⁶/s) Moses and Ta-You Wu, Deb,
$10^{-32}-10^{34}$ Penndorf,
1.5×10^{-32} Bates,
10^{-32} Mitra [17].

We take κ_2 to be 10^{-32}cm⁶/s and κ_1 to be $10^{-18}-10^{-20}$cm³/s and 10^{-21}cm³/s for two cases noted above respectively. Then

$$r=(10^{-14}\sim10^{-13})n(1-\theta),$$

or $$r=10^{-11}n(1-\theta).$$

Thus the recombination by two body collision is predominent above the level where the concentration of the total particle is at least 10^{11}/c.c..

Appendix II

(a) The Range of the Dissociation of Nitrogen for Application of (26).

If we assume that

$$[N]=\frac{h-h_0}{a}[N_2]=\frac{h-h_0}{a}[N_2]_0 e^{-\frac{1}{H_{N_2}}(h-h_0)}, \quad H_{N_2}=\frac{kT}{2m_N g}, \tag{45}$$

then

$$\int_{h_0}^{\infty}[N]dh=\int_{h_0}^{\infty}\frac{h-h}{a}[N_2]_0 e^{-\frac{1}{H_{N_2}}(h-h_0)}=\frac{[N_2]_0}{a}(H_{N_2})^2, \tag{46}$$

where a is constant, $[N_2]_0$ is the value at h_0 and the upper limit is taken as infinitive instead of $h=h_0+a$, for convenience of computation.

Then
$$\int_{h_0}^{\infty}[N_2]dh\simeq[N_2]_0 H_{N_2}, \tag{47}$$

and
$$QH_N=2H_{N_2}[N_2]_0. \tag{48}$$

Hence
$$QH_N\Big/\int_{h_0}^{\infty}[N]dh=\frac{2a}{H_{N_2}}. \tag{49}$$

When $a=100$km and $H_{N_2}=10$km (49) becomes

$$\int_{h_0}^{\infty}[N_2]dh \Big/ \int_{h_0}^{\infty}[N]dh \simeq 10, \quad QH_N \Big/ \int_{h_0}^{\infty}[N]dh = 20.$$

If h_1 is the level of ten percent dissociation,

then $$\int_{h_1}^{\infty}[N_2]dh \Big/ \int_{h_1}^{\infty}[N]dh \simeq 5, \; Q_{h_1}H_N \Big/ \int_{h_1}^{\infty}[N]dh = 10.$$

(b) The Range of the Dissociation of Nitrogen for Application of (30).

If we assume

$$[N_2]=[N_2]_0 e^{-\frac{h-h_0}{H_{N_2}}}, \tag{50}$$

then $$\int_{h_0}^{\infty}[N_2]=H_{N_2}[N_2]_0. \tag{51}$$

If degree of dissociation is fifty percent at h_2,

$$H_N Q = 4H_{N_2}[N_2]_0, \tag{52}$$

and $$\int_{h_2}^{\infty}[N_2]dh/H_N Q = \frac{1}{4}. \tag{53}$$

As it is estimated that $[N_2]$ decreases more rapidly than that expressed by (50), the ratio in (53) becomes smaller. Hence it seems that above the level of dissociation of fifty percent (30) approximately holds.

References

(1) H. Rakshit, Ind. J. Phys., **21**, 57 (1947)
(2) R. Penndorf, J. Geophys. Resear., **54**, 7 (1949)
(3) H.E. Moses and Ta-You Wu, Phys. Rev. **83**, 109 (1951)
(4) The Rocket Panel, Phys. Rev., **88**, 1027 (1952)
(5) D.R. Bates and H.S.W. Massey, Proc. R. Soc., A, **187**, 261 (1946)
(6) D.R. Bates, Ann. de Geophys., **8**, 194 (1952)
(7) S.K. Mitra, Nature, **167**, 897 (1951)
(8) G. Herzberg and L. Herzberg, Nature, **161**, 283 (1948)
(9) S. Deb, J. Atmosph. Terr. Phys., **2**, 309 (1952)
(10) D.R. Bates and M.J. Seaton, Proc. Phys. Soc., B, **63**, 129 (1940)
(11) M. Nicolet, J. Geophys. Resear., **54**, 373 (1940)
(12) M. Nicolet, Ins. Ass. Terr. Mag., Oslo, 1948, Document T 58 (1951)
(13) H.K. Callmann, J. Geophys. Resear. **58**, 209 (1953)
(14) D.R. Bates, Proc. R. Soc. A, **196**, 562 (1949)
(15) G. Herzberg, Astrophys. J. **89**, 290 (1939)
(16) M. Nicolet, Ins. Roy. Met. Belgique, Mem., **19**, (1949)
(17) S.K. Mitra, The Upper Atmosphere, The Asiatic Society, Calcutta (1952)

Propagation of the Cosmic Radiation through Interstellar Space

By Saito HAYAKAWA and Shinsaku KOBAYASHI

Department of Physics, Osaka City Univervsity

Department of Physics, Osaka University

Abstract

Various theories on the origin of the cosmic radiation are critically surveyed. Expected phenomena resulting from the galactic origin theory in which charged cosmic rays are trapped by the glactic magnetic field are discussed with special regard to the secondaries due to the collisions with interstellar hydrogen. Electrons through the decay process $\pi \to \mu \to e$ are then expected to amount 3~9% of the total intensity, depending upon the magnetic field strength in our galaxy. An alternative hypothesis that the cosmic radiation propagates in a straight way is also examined. It is proposed that this may be tested by observing primary photons, resulting from the decay process $\pi^0 \to 2\gamma$, which could be several percent of the total radiation at low latitudes.

1. Introduction

It has been thought plausible that the cosmic radiation is stored in a finite region of the universe, since otherwise the amount of energy carried by the cosmic radiation is far larger than that by the electromagnetic radiation that might be a source of the former energy. This has, on one hand, led Richmyer and Teller (1) to their speculation that the cosmic radiation is confined only in the solar system, and, on the other hand, Fermi (2) and Unsöld (3) to their theories of its galactic origin,*) where the cosmic radiation is kept inside due to the wandering magnetic field suggested by Alfvén (4).

Although these theories are ingeniously elaborated, a number of difficulties have been poined out. The solar origin does hardly harmonize with the unappreciable diurnal variation of very energetic cosmic rays which can not so much curl in the magnetic field as to be made isotropic (5). The galactic origin, though interesting in view of their acceleration mechanism, meets an objection, when experiments on heavy primaries are taken into consideration. A negligible amount of Li, Be and B in the primary cosmic radiation observed by Bradt and Peters (6) led them to conclude the small thickness ($\lesssim 2 \mathrm{g\,cm^{-2}}$) of matter traversed by the cosmic radiation from its origin to the top of the atmosphere, while the galactic origin theory requires the

*) By the galactic origin we mean that the cosmic radiation is created in our galaxy and stored in it, if not specially noticed.

thickness of traversed matter as large as the absorption mean free path of cosmic rays ($\sim 40\,\mathrm{g\,cm^{-2}}$).

The scarcity of Li, Be and B is, however, opposed by a later experiment by Daniton *et al* (7) who observed as many Li, Be and B as C, N and O. This allows the thickness of traversed matter to be larger, but its upper limit is set by the existence of heavier nuclei whose absorption mean free path is about $10\,\mathrm{g\,cm^{-2}}$. Thus the contradiction with the galactic origin hypothesis is yet unsolved, irrespective to whether the abundance of Li, Be and B are appreciable or not.

Although these experimental results are unfavourable to the galactic origin, it seems worth while to seek for further evidences for or against this hypothesis. This is our principal aim of this paper, a preliminary account being published in a previous short note (8).

2. Diffusion of the Cosmic Radiation in the Galaxy

According to Fermi (2) and Unsöld (3), cosmic ray particles are scattered by magnetic clouds whose linear dimension, L, is of the order of 10^{17}cm (Fermi) or 10^{20}cm Unsöld. If the cosmic radiation is created at $r=0$ with unit intensity, its density at r after time t is given by (9)

$$\rho(r,t)=(2\pi\lambda^2)^{-3/2}\exp\{-(r^2/2\lambda^2)-t/T\}, \tag{2.1}$$

where the boundary condition is natural and different from that assumed by Cocconi (5). λ is the diffusion length and is related with the number of collisions with magnetic clouds, N, as

$$\lambda^2=2NL^2/3=2ctL/3. \tag{2.2}$$

T is the mean life time due to the colliisons with interstellar matter, mainly with hydrogen of density 1 atom $\mathrm{cm^{-3}}$.

With the collision cross section for protons $\sim 5\times10^{-26}\mathrm{cm^2}$,

$$T=7\times10^{14}\mathrm{sec}=2\times10^{7}y.^{*)} \tag{2.3}$$

For an instanteneous source, such as suggested by Sekido *et al* (10) the density reaches the maximum at

$$t=\frac{3}{4}T\{\sqrt{1+4r^2/3cLT}-1\}. \tag{2.4}$$

In Sekid's example, the coimic radiation would have been originated 1.2×10^{11}sec ago at 3×10^{21}cm apart from the earth (at the Grab nebula). Then the cosmic radiation would be far before its mean age and its intensity would be increasing with rate $3c/4L$, corresponding to $0.2\%\,y^{-1}$ for $L=10^{20}$cm. Thus the contradiction between Sekido's (10) and Cornell's (5) (11) results should not be due to the difference in the periods of observation if Sekido's conjecture were approved.

The density distribution (2.1) results in anisotropy of the cosmic ray intensity

$$-(L/3)\nabla\rho/\rho=r/2ct. \tag{2.5}$$

*) The absorption mean free path may be only slightly different from the collision mean free path in such diffuse matter, where pions taking main part in N-cascades at high energies undergo decays before collisions.

This leads in Sekido's example to the anisotropy of about 3/8, which is, of course, covered by a large background. If the observed anisotropy of about 10% were true, the Crab nebula should contribute to the total intensity by nearly 2%. Since the contribution is far before its maximum at the present, its contribution would be unreasonably large in future. If the explosions of supernovas such as the Crab nebula were to account for the whole intensity of cosmic rays (12), the explosions of every 300 y would result in too large intensity to be consistent with our experiences, provided Sekido's work were to be acceptable.

If the cosmic radiation is continuously produced with a constant intensity, that produced at T before gives the largest contribution. For such a source locating at the center of our galaxy, the anisotropy is expected to be about 0.07% which may be too small to be detectable by present techniques. It may be noteworthy that the maximum of the cosmic ray intensity expected is just in an opposite side of the observed one (13), though the observation on siderial time variations is not conclusive yet.

There could be another cause of anisotropy, if the source is at the center. Since the solar system flies away from the center with the velocity of about 3×10^6cm sec^{-1}, the intensity at the opposite side could be larger than that at the side of the center by about 0.02%. This is again too small to be observed. As seen above, the cosmic radiation should distribute practically isotropic in the galaxy, independent of its positions of sources, so that the uniform density may be assumed in the following qualitative discussions. Then the density distribution (2.1) contains only a time dependent factor exp $(-t/T)$.

Now we consider the secondaries produced by the collisions of primaries with interstellar hydrogen. The density of the secondaries is given by

$$f\frac{T_2}{T-T_2}(e^{-t/T}-e^{-t/T_2}), \tag{2.6}$$

where T_2 represents the mean life of secondaries and f the fractional intensity of secondaries produced per collision with the same energy as the incident primary. For large t when the equilibrium between primaries and secondaries is reached, the ratio of secondaries to primaries tends to

$$fT_2/T. \tag{2.6'}$$

This is employed by Bradt and Peters (1) in estimating the contribution of heavy primaries.

So far we have assumed that the cosmic radiation originates solely in the galaxy. The case may be plausible where a part of the cosmic radiation comes from out of our galaxy and is trapped due to the galactic magnetic field. Assuming that the intensity outside the galaxy is I_0 and a fraction, g, of the cosmic radiation striking the galactic surface can penetrate, the density inside the galaxy follows the equation

$$\frac{d\rho}{dt}=-\left(\frac{1}{T}+\frac{cS}{2V}g'\right)\rho+2\pi\frac{S}{V}gI_0, \tag{2.7}$$

where S and V are the surface area and volume of the galaxy, respectively, and a term $cSg'/2V$ expresses leakage through the galactic surface. (2.7) is solved as

$$\rho=2\pi(S/V)gI_0T_1(1-e^{-t/T_1}) \tag{2.8}$$

with

$$1/T_1=1/T+cSg'/2V. \tag{2.9}$$

For large t this tends to

$$\rho=2\pi(S/V)gI_0T_1=s\,g\rho_0, \tag{2.10}$$

where $\rho_0=4\pi I_0/c$ is the density outside and $s=cT_1S/2V$ may be called the storage factor after Unsöld (3). On account of (2.9) the storage factor is given by

$$s=s_0/(1+s_0\,g'), \tag{2.11}$$

where $s_0=cTS/2V$ is the storage factor without leacage. Since s_0 is of the order of 10^3, the density inside is much larger than that outside, provided $s_0g'<1$. Then sources outside contribute to the observed intensity by an unappreciable amount and the supernova origin theory (12) would have to be reexamined for being reconciled with the galactic magnetic field hypothesis.

3. Secondaries Produced by the Collisions with Interstellar Matter

The collisions of heavy nuclei with interstellar matter have been discussed by Bradt and Peters (1). Fan (9) argued that this process could account for the observed abandunce of heavy nuclei with the acceleration mechanism proposed by Fermi (2). The energy spectra they obtained should be steeper, the heavier the nuclei are, in contradiction with recent observations (14) (15). This is another difficulty against the galactic origin. Further difficlties are found if other possible secondaries are taken into consideration, as will be shown in what follows.

Since most of the primary cosmic radiation are protons, it may be sufficient for our purpose to deal with the collisions of protons with interstellar hydrogen. As the order of magnitude theory, the intensities of secondaries may be estimated in considering the minimum energy of primaries responsible to the production of the secondaries under consideration, as has been done in our previous note (8). In this method of estimate was assumed the energy spectrum of the secondaries not appreciably different from that primaries. This is really a good approximation at high energies and for the processes we consider. For the purpose of definiteness, however, we shall calculate the spectra as well as intensities of secondaries in reference to Fermi's theory of multiple meson production (16), though the theory is only tentative and other theories of meson production lead us to similar conclusions.

For later purposes we are mainly concerned with thin interstellar matter and the cascade development of protons is discarded.*) Then the energy spectrum of protons changes so little that we may assume the spectrum everwhere to be the same as that observed at the top of the atmosphere. This is given at high energies in a good approximation by (15)

$$p(E)dE=p_0E^{-\beta}dE, \tag{3.2}$$

*) See also footnote at page 84

where E is the total energy of a proton and $\beta=2.0\sim2.5$ gradually increasing with energy. The use of such a power spectrum is suggested by analytical convenience.

Secondaries produced by proton-proton collisions are protons, neutrons and their anti-particles, if exist, and also various mesons. Among them only protons, anti-protons, electrons, positrons and photons are stable, the latter three being dacay products.

(a) Anti-protons. The search for anti-protons in the primary cosmic radiation would provide an interesting test for or against their existence, if their intensity were high enough. In the galactic origin theory, their intensity is expected to be f times of the intensity of protons, because $T_2=T$ in (2.6). There are neither reliable experiment nor trustable theory for the magnitude of f, however. We can only set an upper limit of the intensity based on a primitive consideration.

The threshold energy for producting an anti-proton is 8 Gev. Near the threshold, however, the volume of momentum space of the final state is so small that the cross section is expected to be very small. The cross section may reach as large as the geometrical one only above 100 Gev. Thus their intensity is at most of the order of 1% of the proton intensity. Taking into account the competition with the production of mesons, the actual intensity may be a fraction of percent. Hence the existence of anti-protons could hardly be examined.

(b) Electrons (positrons inclusive). Neutrons are possible to contribute to electrons through their β-decays, but the energy imparted to an electron is so small that they are neglected in comparison with other processes. The largest contribution comes from charged pions through muons, while other unstable particles may contribute to small percentage.

For comparsion with the latest experiment at geomagnetic latitude 55° (17), we estimate the minimum energy of primary protons contributing to electrons whose cut off energy is 1.7 Gev. Since an electron takes on the average 1/3 of the energy of a parent moun, the minimum energy of muons under consideration may be taken as about 5 Gev. Those muons are the decay products of pions with energy greater than 6 Gev, because the average energy of a muon is about 0.8 times an energy of a parent pion. If n pions with average energy E_π are produced by a proton of energy E, there holds a relationship

$$2\gamma(\gamma-1)\geqq nE_\pi, \tag{3.2}$$

provided pions are produced istropically in the center of mass system. γ is the Lorentz factor that transforms the laboratory system into the center of mass system and is expressed as

$$\gamma=\sqrt{(E+1)/2}, \tag{3.3}$$

where the total energy E is measured in unit of proton rest energy. Then we obtain $E>10$ Gev for $n=1$, $E>17$ Gev for $n=2$ and so forth. For $E=10\sim20$ Gev the average number of pions produced may be two. Hence we can roughly set the minimum energy of protons for producing observable electrons as

$$E\gtrsim 20\,\text{Gev}, \quad (\pi-\mu-e), \tag{3.4}$$

taking into account recoils of colliding protons. This gives to fraction f in (2.6)

$$f \lesssim 0.05, \quad (\pi-\mu-e) \tag{3.5}$$

for $\beta = 2.0$ in (3.1). Thus the intensity of electrons would be appreciable, if protons were to traverse thick enough intersteller matter.

A more quantitative estimate is carried out in reference to the Fermi's theory of meson production and to a power spectrum like (3.1). The differential spectrum of electrons is obtained as

$$h_0(E_e, t)\,dE_e = 0.080\,p_0(1-e^{-t/T})\,E_e^{-2(2\beta-1)/3}\,dE_e. \tag{3.6}$$

E_e is the energy of an electron in unit of proton rest energy. The intensity of the electrons is obtained by integrating (3.6) above a magnetic cut-off energy E_e^c as

$$H_0(E_e^c, t) = (0.24/(4\beta-5))\,p_0(1-e^{-t/T})\,E_e^{c-(4\beta-5)/3}. \tag{3.7}$$

Thus the ratio to the intensity of protons is given for $E_e^c = 1.8$ as

$$f_e = \begin{cases} 0.044 & (\beta=2.0), \\ 0.017 & (\beta=2.5). \end{cases} \tag{3.8}$$

These figures are in rough agreement with (3 5).

If the electrons thus produced are trapped by our galaxy with mean life time T_2 their intensity is given by (2.6) with (3.8). The mean life time T_2 is subjected to the interactions of electrons with galactic electromagnetic wave, as discussed by Feenberg and Primakoff (8) and elaborated by Donahue (19). According to their investigations the most important process for the energy loss of electrons is the Compton collisions with galactic photons.

Since both the cross section and energy loss for the Compton process decrease above the electron rest energy mc^2, only the nonrelativistic limit in the rest system of an electron may be considered. Then the cross section is that for the Thomson scattering and the energy loss is $\xi^2\epsilon$, where ϵ and ξmc^2 is the energies of colliding photon and electron in the observed system. With the energy spectrum of photons $n(\epsilon)\,d\epsilon$, the energy loss of an electron is approximately evaluated as

$$\begin{aligned} dE_e/dt &= -c\sigma_c \int_0^{mc^2/\xi} n(\epsilon)\,\xi^2\epsilon\,d\epsilon, \\ \sigma_c &= (8\pi/3)(e^2/mc^2)^2. \end{aligned} \tag{3.9}$$

On account of that $n(\epsilon)\,\epsilon\,d\epsilon$ is the differential energy density spectrum, the energy loss (3.9) is proportional to the energy density of photons with energies below mc^2/ξ. Hence

$$\begin{aligned} dE_e/dt &= -c\sigma_c\xi^2 W(mc^2/\xi) = -2\times 10^{-14}\xi^2 W(mc^2/\xi)\,\mathrm{ev\,sec^{-1}}, \\ W(mc^2/\xi) &= \int_0^{mc^2/\xi} n(\epsilon)\,\epsilon\,d\epsilon. \end{aligned} \tag{3.10}$$

$W(mc^2/\xi)$ may be equated to the energy density of galactic photons. This is about 0.3 ev/cc for visible light and the order of 10^{-5}ev/cc for radio frequency

radiation. Hence only the visible light is taken into consideration.

The life time for an electron of energy $\xi_0 mc^2$ losing its energy down to ξmc^2 is then obtained as

$$T_e = 5\times 10^{13}(mc^2/W)(1-\xi/\xi_0)/\xi \text{ sec.} \tag{3.11}$$

For $\xi_0 mc^2 = 10$ Gev and $\xi mc^2 = 5$ Gev

$$T_e \simeq 4\times 10^{15} \text{ sec.} \tag{3.11'}$$

This is larger than the mean life time of protons.

We may, therefore, expect a considerable intensity of electrons with energies below 10 Gev in the primary cosmic radiation. The differential energy spectum of such electrons that are produced by the collisions of protons with interstellar hydrogen and suffer the collisions with galactic photons can be obtained by solving a diffusion equation

$$\frac{\partial h(E_e, t)}{\partial t} = k_c \frac{\partial E_e^2 h(E_e, t)}{\partial E_e} + S(E_e, t). \tag{3.12}$$

$k_c E_e^2$ is the energy loss given by (3.10) with

$$k_c = c\sigma_c W/(mc^2)^2 \simeq 2\times 10^{-25} \text{ev}^{-1}\text{sec}^{-1}. \tag{3.10'}$$

The continuous energy loss adopted above may be permitted on account of that several Compton collisions take place in the mean life time of an electron and the energy loss per collision is much smaller than E_e in our case. The source of electrons, $S(E_e, t)$, is taken from (3.6) in an equilibrium state as

$$S(E_e, t) = (S_0/T)E_e^{-u},$$
$$u = 2(2\beta-1)/3. \tag{3.6'}$$

The diffusion equation is soved as

$$h(E_e, t) = S_0 E_e^{-u-1}/k_c(u-1). \tag{3.13}$$

The intensity of electrons is obtained by integrating (3.13) for E_e larger than the cut-off energy, E_e^c.

$$H(E_e^c) = S_0 E_e^{c-u}/k_c u(u-1). \tag{314}$$

The ratio to the intensity of protons is about 0.09 for $E_e^c = 1.8$ and $\beta = 2.0$, which is large enough to be detectable.

If there were strong magnetic fields in our galaxy, the radiation loss of electrons due to curling in the magnetic field would not be negligible either.*) The radiation loss of an electron with energy E_e in a magnetic field of strength H (in gauss) is given by

$$\frac{dE_e}{dt} = -1\times 10^{-3} H^2 \xi^2 \text{ev sec}^{-1}. \tag{3.15}$$

Since this process has the same energy dependence as the energy loss by the Compton effect, one has only to add a term k_H to k_e. Comparing (3.15) with (3.10), and (3.10'), we have

*) The authors are grateful to Professor Rossi for callidg our attention to this process.

$$k_H = 1\times10^{-3}H^2/(mc^2)^2 \simeq 4\times10^{-15}H^2 \text{ev}^{-1}\,\text{sec}^{-1}. \tag{3.15'}$$

Hence for $H\simeq7\times10^{-6}$ gauss the radiation loss is comparable with the loss by the Compton effect. For the maximum possible magnetic field strength, 10^{-5} gauss, $k_H = 4\times10^{-25}$ results in the reduction of the intensity of electrons by a factor of three in comparison with the above estimate. In this case electrons should be barely dectable in the primary cosmic radiation.

The absence of electrons in the primary cosmic radiation is, therefore, found to be a clue to testify the galactic origin. There might, however, be ambiguities in the above estimate, although all but the density of galactic photons do not seem to depress the ratio of the electron intensity to the proton intensity below 1%. We have assumed the photon density as uniform throughout the galaxy, but it is merely a rough approximation. If the electrons spend more time in strong magnetic fields where the density of photons might be larger than in other parts, the intensity of eletrons would be smaller than that given above and our argument would have to be reviced. In this case, however, the evidence on heavy primaries remains to be against the galactic origin.

(c) Photons. In the experiment referred (17) photons of energies greater than 0.73 Gev are tried to observe. The energy of a neutral pion which produce photons of this energy is about 1.5 Gev. This pion can be produced by a proton of energy above 3 Gev. Taking into account the recoil of nucleons, the minimum energy of the protons responsible to the observable photons may be assumed as 4 Gev. Hence their intensity at 55° is about 1/2 of the total proton intensity. Around this energy most of pions are produced singly and 1/3 of them may be neutral. Thus we obtain the fraction of observable photons per proton-proton collision as

$$f_\gamma \simeq (2/3)\times(1/2)\simeq 0.3. \tag{3.16}$$

More quantitative estimate is made in reference to Fermi's theory as in (b). The differential spectrum of photons is evaluated as

$$g(E_\gamma)\,dE_\gamma = 0.35\,p_0(1-e^{-t/T})E_\gamma^{-2(2\beta-1)/3}dE_\gamma. \tag{3.17}$$

Integrating (3.16) above the cut-off energy $E_\gamma{}^c$ that depends upon experimental conditions, we obtain the intensity of photons

$$G(E_\gamma{}^c) = \frac{1.05}{4\beta-5}p_0(1-e^{-t/T})E_\gamma{}^{c-(4\beta-5)/3}. \tag{3.18}$$

For $E^c = 0.8$

$$f_\gamma = \begin{cases} 0.4 & (\beta=2.0), \\ 0.3 & (\beta=2.5). \end{cases} \tag{3.19}$$

In order to account for the intensity of the photons which are in equilibrium with protons, we must modify (2.6), since photons are not trapped by the magnetic field. The mean life time for photons is now estimated on account of escaping of photons out of our galaxy as

$$T_{2,\gamma}=2V/cS\simeq 10^{12}\,\text{sec.} \tag{3.20}$$

Hence the fractional intensity of photons is given by

$$f_\gamma(T_{2,\gamma}/T)\simeq 5\times 10^{-4}, \tag{3.21}$$

which is too small to be detectable.

From the above discussions we could expect the detectable intensity of electrons against observations if there were such a galactic magnetic field trapping charged particles that were not too strong. Together with other evidences mentioned in Section 1, doubt may be thrown upon the existence of such a magnetic field as well as the theories of Fermi and Unsöld. It seems now necessary to examine the hypothesis that the cosmic radiation propagates in a straight way through the galaxy. How one can test the latter presumption will be considered below.

4. Possible Observable Effects for the Cosmic Radiation Going in a Straight Way through the Galaxy

Under this assumption we may expect the anisotropy of the cosmic radiation, since the earth locates near the edge of our galaxy and the amount of matter traversed is different depending upon the incident direction. At siderial time 18h the cosmic radiation traverses the thickest matter of about $0.5\,\text{g/cm}^2$. This results in the absorption of several percent for heavy neclei. In practical cases the finite solid angle of an apparatus makes this percentage as small as the order of 1%.

As for secondaries such as electrons and photons, (2.6) is applied only at small t, so that their intensity is given by

$$fx/\lambda \tag{4.1}$$

where x is the thickness traversed in g cm^{-2} and λ is the collision mean free path for primaries. For protons traversing through the center of the galaxy, $x/\lambda=0.5/30\simeq 0.02$. Now we can estimate the intensity of various secondaries as in Section 3.

(a) Anti-protons. f is only the order of 1% so that this is out of question.

(b) Electrons. This case is nothing to do with the absorption as discussed in Section 3. Thus electrons are expected to be practically unobservable either.

(c) Photons. Now the large f_γ in (3.19) is of considerable importance. At 55° where the cut-off energy for protons is low, the intensity of photons is at most a fraction of percent, in cosistent with the observation (17). At low latitudes, hewever, the intensity of charged primaries decreases, whereas the intensity of photons remains unchanged. Then the relative intensity of photons increases with decreasing latitude and could be several percent of the total primary intensity at the equator. This is certainly observable by the present evperimental techniques. The directional dependence or the diurnal variation of photon intensity may also be observable.

5. Concluding Remarks

We have considered the various effects of collisions of the cosmic radiation with interstellar matter. On the basis of the galactic origin theory that charged particles are stored in our galaxy, a difficulty arises on account for the negligible intensity of

electrons which should be produced by the collisions with interstellar matter and trapped by the galactic field, though this evidence has to be taken with reservation. This and other difficulties regarding with heavy primaries may be unfavourable to the presence of the galactic magnetic field that traps charged cosmic rays for long periods, though an astrophysical evidence is reported for supporting its presence (20).

An alternative hypothesis that the cosmic radiation is not stored in our galaxy but comes mainly from other galaxies seems rather plausible. In order to see whether this hypothesis is acceptable or not, the observation of photons in primary cosmic rays at low lattitudes is suggested.

If this is approved, we shall have to turn towards the nonequilibrium theory of the cosmic radiation, as often presumed by Lemâitre (21) and others, because it takes as long time as the age of the universe that the cosmic radiation travels from the farthest galaxies to the earth. Then the composition and the energy spectrum of the cosmic radiation might be correlated with the origin of the universe. The difference in the compositions of cosmic rays and existing elements may be attributed to the acceleration of the former due to the gravitation effect that should be of greatest importance at the origin of the universe and is more effective for heavier elements. The electromagnetic acceleration is proportional to Z/A in ordinary conditions and hardly account for more abundant high Z elements in the cosmic radiation than in whole elements and for the unexpectedly large energy content of the cosmic radiation.

References

(1) R.D. Ritchtmyer and E. Teller, Phys. Rev. **75**, 1729 (1949)
(2) E. Fermi, Phys. Rev. **75**, 1169 (1949)
(3) A. Unsöld, Phys. Rev. **82**, 857 (1951)
(4) H. Alfvén, Cosmical Electrodynamics (1949)
(5) G. Cocconi, Phys. Rev. **83**, 1193 (1951)
(6) H.L. Bradt and B. Peters, Phys. Rev. **77**, 54 (1950); **80**, 943 (1951)
(7) A.D. Dainton, P.H. Fowler and D.W. Kent, Phil. Mag. **42**, 317 (1951); **43**, 729 (1952)
(8) S. Hayakawa, Prog. Theor. Phys. **8**, 571 (1952)
(9) C.Y. Fan, Phys. Rev. **82**, 211 (1951)
(10) Y. Sekido, T. Masuda, S. Yoshida and M. Wada, Phys. Rev. **83**, 658 (1951)
(11) P.H. Barrett and Y. Eisenberg, Phys. Rev. **85**, 672 (1952)
(12) D. ter Haar, Rev. Mod. Phys. **22**, 119 (1950)
(13) H. Elliot, Progress in Cosmic Ray Physics, **1**, 452 (1952)
(14) M. Kaplon, B. Peters, H.L. Reynolds and D.M. Ritson, Phys. Rev. **85**, 295 (1952)
(15) P.H. Barret et al., Rev. Mod. Phys. **24**, 133 (1952)
(16) E. Fermi, Prog. Theor. Phys. **5**, 570 (1950); Phys. Rev. **81**, 683 (1951)
(17) C.L. Critchfield, F.P. Ney and S. Oleska, Phys. Rev. **85**, 461 (1952)
(18) E. Feenberg and H. Primakoff, Phys. Rev. **72**, 449 (1948)

(19) T.M. Donahue, Phys. Rev. **84**, (1951)
(20) W.A. Hilther, Astrophys. J. **114**, 241 (1951)
(21) G. Lemâitre, Rev. Mod. Phys. **21**, 357 (1949)

The Vertical Distribution of Electrical Conductivity in the Upper Atmosphere*

By Hiroshi MAEDA

(Geophysical Institute, Kyoto University)

Abstract

Using available materials of recent rocket measurements, a calculation is made to obtain the atmospheric and ionospheric models of the upper atmosphere between 60km and 400km. On the basis of these models the vertical distribution of electrical conductivity and its height-integrated values for three ionospheric regions *F*, *E* and *D* are obtained. The results show that the conductivity of the *E*-region, especially near 100km, is most predominant, so that this region is most probably effective to the electrical currents producing daily magnetic variations.

1. Introduction

Recently, from four sources [1] anisotropic conductivity of the upper atmosphere has been proposed simultaneously. This new concept of conductivity plays probably an important role in the electromagnetic interpretation of the problems relating to the upper atmosphere. Therefore, it needs to try a detailed calculation to obtain the vertical distribution of conductivity in the upper atmosphere. For this purpose, however, the atmospheric and ionospheric models must be determined.

Since 1946, a relatively great number of sounding rockets have been fired in order to obtain direct information on pressure, density and temperature of the upper atmosphere. From these results the Rocket Panel [2] has reported a combined result, and given two tables of physical properties of the atmosphere up to 220km. Recently H.K. Kallmann [3] has studied theoretically the physical state of the atmosphere between 80km and 250km, and given a table which is in fair agreement with the results of rocket measurements.

Very recently, the results of direct measurements of the electron density in the ionosphere by rocket-borne instruments have been reported by W.W. Berning [4], and J.R. Lien, R.J. Marcou, J.C. Ulwick, J. Aarons, and D.R. McMorrow [5].

In the present paper, the author shows the results of calculation of the vertical distribution of electrical conductivity and its height-integrated values, using atmospheric and ionospheric models deduced from the rocket measurements mentioned above.

---

* Contribution of Geophysical Papers dedicated to Prof. M. Hasegawa on his sixtieth birthday.

2. Atmospheric model

(i) *Temperature* (T)

The vertical distribution of temperature up to 80km follows the result adopted by the Rocket Panel [2], and above 80km the following linear distribution assumed by Kallmann [3] is used:

$$T=T_0+\gamma(h-h_0) \tag{1}$$

where

h_0 = datum level = 80 km

T_0 = temperature at the datum level = 190°K

γ = lapse rate = 2.5°K per km.

The distribution is shown in Fig. 1.

(ii) *Molecular weight* (M)

According to Kallmann [3], if the following assumptions are made:

a) Oxygen dissociates in the region between 80 and ~120km,

b) Nitrogen dissociates in the region between ~130 and 250km,

c) The temperature and pressure at the datum level (80km) are known and the lapse rate is 2.5°K per km,

d) The fractional change in concentration is of the form

$$\frac{dC[O_2 \text{ or } N_2]}{C[O_2 \text{ or } N_2]}=-K_t dh$$

where C is the concentration of molecular oxygen or nitrogen at any height, and K_t is a concentration coefficient equal approximately to $1.93\times10^{-6}\text{cm}^{-1}$ for O_2 and $0.98\times10^{-6}\text{cm}^{-1}$ for N_2,

then the molecular weight as a function of temperature and of height is obtained from the equations

$$\frac{dM_1}{dh}=\left[\frac{M_1-23.8}{T}\right]\left[\frac{M_1 g}{R}+\gamma-K_1 T\right] \tag{2}$$

$$\frac{dM_2}{dh}=\left[\frac{M_2-14.4}{T}\right]\left[\frac{M_2 g}{R}+\gamma-K_2 T\right] \tag{3}$$

where M_1 and M_2 are the mean molecular weight of air in the regions where oxygen and nitrogen dissociates, respectively, and g is the gravity. Also in our calculation, these equations are used, and the result of calculation is shown in Fig. 1.

(iii) *Gravity* (g)

The Distribution of gravity with height is calculated from the inverse square law

$$g=g_0\left(\frac{a}{a+h}\right)^2 \tag{4}$$

where

a = radius of the earth = 6372 km

g_0 = gravity at the earth's surface = 980 cm.sec.$^{-2}$

(iv) *Scale height* (H)

Using above quantities, the scale height can be calculated from the relation

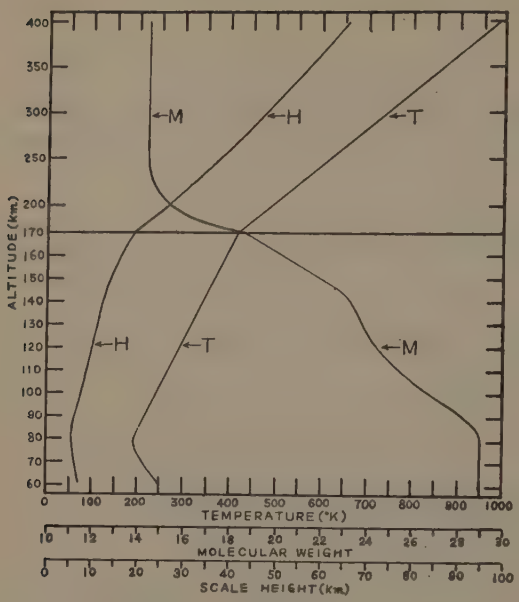

Fig. 1—Altitude *vs* temperature, molecular weight, and scale height.

$$H=\frac{RT}{Mg} \qquad (5)$$

where R is gas constant. The distribution of H is shown in Fig. 1.

(v) *Pressure* (P)

The pressure is obtained by numerical integration of the equation

$$\frac{dP}{P}=-\frac{1}{H}\,dh \qquad (6)$$

(vi) *Density* (ρ)

The density is obtained from the equation of state

$$\rho=\frac{PM}{RT} \qquad (7)$$

(vii) *Number density* (n)

The number density shown in Fig. 2 is calculated from the relation

$$n=\frac{P}{kT} \qquad (8)$$

where k is Boltzmann's constant.

(viii) *Geomagnetic total intensity* (F)

The geomagnetic total intensity is calculated from the inverse cube law

$$F=F_0\left(\frac{a}{a+h}\right)^3 \qquad (9)$$

where F_0 = geomagnetic total intensity at the earth's surface = 0.5 gauss.

3. Ionospheric model

(i) *Electron density* (n_e)

The results of direct measurements of the electron density in the ionosphere mentioned above are fairly complicated, so that, based on these results, we have assumed a model distribution of the electron density at daytime shown in Fig. 2.

(ii) *Ion density* (n_i)

Recently preliminary rather succesful attempts to determine the ionization in the E-region by means of a probe technique are described by

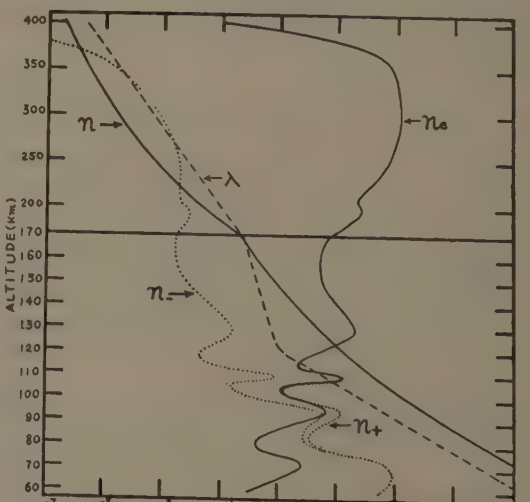

Fig. 2—Altitude *vs* gas density, electron and ion (negative and positive) densities, and negative ion to electron ratio.

Gunner Hok, N.W. Spencer and W.G. Dow [6], and they found that a positive-ion density is about ten times larger than the electron density. This result is very interesting. But, for the purpose of our calculation the height-range of measurements is too small, so that we use a theoretical estimation of λ (the ratio of the concentration of negative ions to that of electrons) by D.R. Bates and H.S.W. Massey [7], until above direct measurements by rocket are extended over all altitudes in the ionosphere.

From theoretical considerations, Bates and Massey have estimated the value of λ in the different ionospheric layers ($F2$-, $F1$-, E-, and D-layers). On the basis of these values, we have assumed the distribution of λ shown in Fig. 2. Using this, the positive and negative ion densities are calculated under the assumption that atmospheric air is electrically neutral as a whole, and these distributions are also shown in Fig. 2.

4. Collision frequency

S. Chapman and T.G. Cowling [8] and T.G. Cowling [9] have given formulae to determine collision frequencies, and recently M. Nicolet [10], using the formulae derived by above authors, has calculated and discussed the electron collision frequency of all ionospheric regions. We follow also these workers.

(a) ***Collision between neutral and charged particles***

In the velocity distribution method, the effective collision interval τ_{12} of molecular mass m_1 and mass m_2 is

$$\tau_{12}=\frac{m_1m_2(n_1+n_2)}{(n_1m_1+n_2m_2)kT}D \tag{10}$$

where D is the ordinary coefficient of mutual diffusion of the two kinds of molecules in the absence of other gases, n_1 and n_2 are the particle number densities, k is Boltzmann's constant, and T is the absolute temperature. To a certain degree of approximation, D is, for rigid elastic sphere,

$$D=\frac{3}{16(n_1+n_2)\sigma_{12}^2}\left[\frac{2kT(m_1+m_2)}{\pi m_1m_2}\right]^{\frac{1}{2}} \tag{11}$$

where σ_{12} is the collision distance.

From (10) and (11), the collision frequency ν_{12} for a molecule of type 1 with molecules of type 2 is

$$\nu_{12}=\frac{16}{3}\frac{n_1m_1+n_2m_2}{m_1+m_2}\pi\sigma_{12}^2\left[\frac{(m_1+m_2)kT}{2\pi m_1m_2}\right]^{\frac{1}{2}} \tag{12}$$

(i) *Collision frequency of an electron with neutral particles* (ν_{en})

For collisions of an electron of mass m_e with neutral particles of mass m with number density n, (12) becomes

$$\nu_{en}=\frac{4}{3}n\pi\sigma_{en}^2\left(\frac{8kT}{\pi m_e}\right)^{\frac{1}{2}} \tag{13}$$

because

$$m_1\equiv m\gg m_e\equiv m_2$$

Thus, the collision frequency of an electron with neutral particles is determined if we can find the effective collision distance. Several workers [9, 10, 11, 12] have calculated ν_{en} using the value of σ_{en} estimated theoretically or experimentally, but it is not easy to obtain an exact value for the collision distance of slow electrons in the ionosphere. We have, therefore, adopted the following relation to obtain ν_{en} as a mean state:

$$\nu_{en}=5\times10^{-10}n\sqrt{T} \tag{14}$$

(ii) *Collision frequency of an ion with neutral particles* (ν_{in})

Assuming that a mass of ions, negative and positive, is equal to a mass of neutral particle, i.e. $m_-=m_+=m$, (12) becomes

$$\nu_{in}=\frac{8}{3}n\pi\sigma_{in}^2\left(\frac{kT}{\pi m}\right)^{\frac{1}{2}} \tag{15}$$

Following Cowling [9], we have used the value

$$\sigma_{in}=5.9\times10^{-8}\left(\frac{300}{T}\right)^{\frac{1}{4}} \tag{16}$$

which is derived from measurements of the mobility of N_2^+ ion in molecular nitrogen by A.M. Tyndall [13], and obtained

$$\nu_{in}=3.35\times10^{-21}\frac{n}{\sqrt{m}} \tag{17}$$

(b) *Collision between charged particles*

According to Chapman and Cowling, the effective collision interval for charged particles of mass m_1 and m_2 is still to be found by (10), but now diffusion coefficient D for charged particles is

$$D=\frac{3}{16}\frac{1}{n_1+n_2}\left[\frac{2kT(m_1+m_2)}{\pi m_1m_2}\right]^{\frac{1}{2}}\left(\frac{2kT}{e^2}\right)^2\frac{1}{A_1(2)} \tag{18}$$

where e denotes the electric charge as used in the following equation for the force P between pairs of particles having charge e_1 and e_2:

$$P=\frac{e_1e_2}{r^2}$$

and $A_1(2)$ denotes a slowly varying function of T and n_e.

(i) *Collision frequency of an electron with ions* (ν_{ei})

If we use the condition

$$m_1\equiv m_i=m\gg m_e\equiv m_2$$

then the collision frequency of an electron with ions of number density n_i is given by

$$\nu_{ei}=\frac{4}{3}\frac{\pi e^4}{(2\pi m_ek^3T^3)^{\frac{1}{2}}}A_1(2)n_i \tag{19}$$

where the correction term $A_1(2)$ is given by Chapman and Cowling as follows:

$$A_1(2)=\log_e(1+v_{01}^2)$$

where

$$\upsilon_{01}=\frac{4dkT}{e^2}$$

with d=mean distance between pair of neighbouring molecules.
If we define d as being equal to Debye's distance, following Nicolet [10],

$$d=\left(\frac{kT}{8\pi e^2 n_e}\right)^{\frac{1}{2}}$$

and if

$$1 \ll \frac{4kT}{e^2(2n_e)^{\frac{1}{3}}}$$

then

$$A_1(2)=2\log_e\frac{4}{\pi^{\frac{1}{2}}e^3 n_e^{\frac{1}{2}}}\left(\frac{kT}{2}\right)^{\frac{3}{2}} \tag{20}$$

Using this correction term, the collision frequency of an electron with ions is given by

$$\nu_{ei}=\left[34+8.36\log_{10}\frac{T^{\frac{3}{2}}}{n_e^{\frac{1}{2}}}\right]n_i T^{-\frac{3}{2}} \tag{21}$$

(ii) *Collision frequency of a negative ion with positive ions* (ν_{-+}), *and of a positive ion with negative ions* (ν_{+-})

Assuming that relation (20) holds in these cases and that $m_-=m_+=m$ for simplicity, then the collision frequencies ν_{-+} and ν_{+-} are given by

$$\nu_{-+}=\frac{3.06\times10^{-14}}{\sqrt{m}}\nu_{e+} \tag{22}$$

$$\nu_{+-}=\frac{3.06\times10^{-14}}{\sqrt{m}}\nu_{e-} \tag{23}$$

Using these, the effective collision frequencies ν_e, ν_- and ν_+ are obtained by

$$\nu_e=\nu_{en}+\nu_{e-}+\nu_{e+} \tag{24}$$

$$\nu_-=\nu_{-n}+\nu_{-+} \tag{25}$$

$$\nu_+=\nu_{+n}+\nu_{+-} \tag{26}$$

and the distributions are shown in Fig. 3.

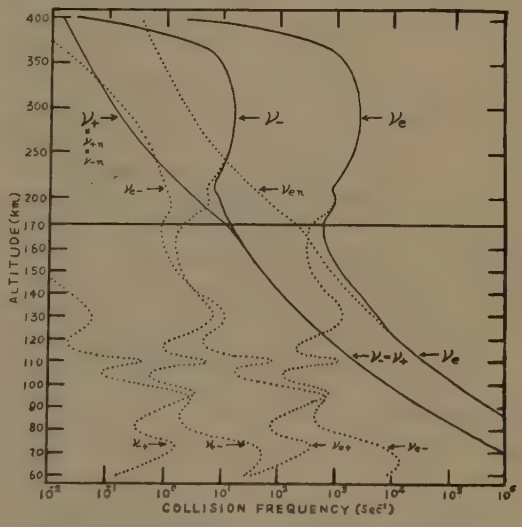

Fig. 3—Altitude *vs* collision frequencies.

5. Electrical conductivity

Using the quantities prepared above, we can calculate the conductivity as below.

(i) According to M. Hirono [14] and D.F. Martyn's [15] expressions, if $\boldsymbol{E}$ may be resolved into components $\boldsymbol{E}_0$ and $\boldsymbol{E}_1$ respectively parallel and perpendicular to $\boldsymbol{H}$ and $\boldsymbol{h}$ is a unit vector parallel to $\boldsymbol{H}$, then the current density is expressed as

$$\boldsymbol{J}=\sigma_0\boldsymbol{E}_0+\sigma_1\boldsymbol{E}_1+\sigma_2(\boldsymbol{h}\times\boldsymbol{E}) \tag{27}$$

where

$$\sigma_0=e^2\left(\frac{n_e}{m_e\nu_e}+\frac{n_-}{m_-\nu_-}+\frac{n_+}{m_+\nu_+}\right) \tag{28}$$

$$\sigma_1 = e^2\left(\frac{n_e}{m_e}\frac{\nu_e}{\nu_e^2+\omega_e^2}+\frac{n_-}{m_-}\frac{\nu_-}{\nu_-^2+\omega_-^2}+\frac{n_+}{m_+}\frac{\nu_+}{\nu_+^2+\omega_+^2}\right) \tag{29}$$

$$\sigma_2 = \frac{e}{F}\left(\frac{n_e\omega_e^2}{\nu_e^2+\omega_e^2}+\frac{n_-\omega_-^2}{\nu_-^2+\omega_-^2}-\frac{n_+\omega_+^2}{\nu_+^2+\omega_+^2}\right) \tag{30}$$

with

$$\omega_e=\frac{eF}{m_e},\quad \omega_-=\frac{eF}{m_-},\quad \omega_+=\frac{eF}{m_+}$$

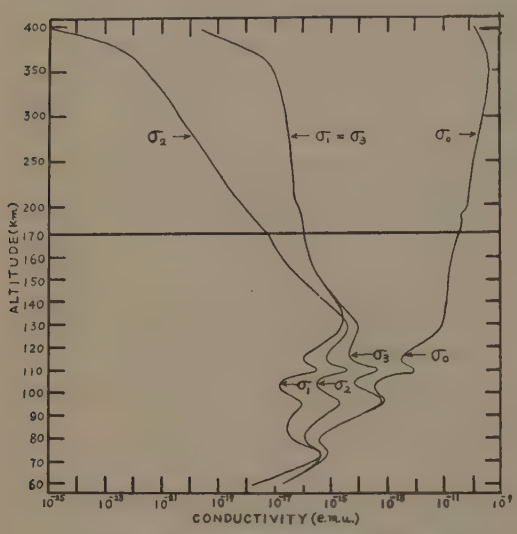

Fig. 4—Altitude *vs* electrical conductivities.

At the magnetic equator, if an eastward electric field is impressed, then the Hall current due to this is vertical, and so makes charges accumulate above and below the conducting layer. If they build up until the resulting vertical polarization field stops further flow of the Hall current, the resultant eastward conductivity is increased to $\sigma_3\left(=\sigma_1+\frac{\sigma_2^2}{\sigma_1}\right)$. Fig. 4 shows the variation of σ_0, σ_1, σ_2, and σ_3 with height.

(ii) Let x-, y-, z- axes be taken to magnetic south, east and upward, respectively, then the current density $\boldsymbol{J}$ is resolved as follows [15]:

$$J_x=(\sigma_0\cos^2\phi+\sigma_1\sin^2\phi)E_x+\sigma_2E_y\sin\phi+(\sigma_0-\sigma_1)E_z\cos\phi\sin\phi \tag{31}$$

$$J_y=-\sigma_2E_x\sin\phi+\sigma_1E_y+\sigma_2E_z\cos\phi \tag{32}$$

$$J_z=(\sigma_0-\sigma_1)E_x\cos\phi\sin\phi-\sigma_2E_y\cos\phi+(\sigma_0\sin^2\phi+\sigma_1\cos^2\phi)E_z \tag{33}$$

where ϕ is the magnetic dip angle.

Assuming that $J_z=0$ at any height in the ionosphere, then

$$E_z=\frac{\sigma_2E_y\cos\phi-(\sigma_0-\sigma_1)E_x\cos\phi\sin\phi}{\sigma_0\sin^2\phi+\sigma_1\cos^2\phi} \tag{34}$$

so that, we have

$$J_x=\sigma_{xx}E_x+\sigma_{xy}E_y \tag{35}$$

$$J_y=-\sigma_{xy}E_x+\sigma_{yy}E_y \tag{36}$$

where

$$\sigma_{xx}=\frac{\sigma_0\sigma_1}{\sigma_0\sin^2\phi+\sigma_1\cos^2\phi} \tag{37}$$

$$\sigma_{xy}=\frac{\sigma_0\sigma_2\sin\phi}{\sigma_0\sin^2\phi+\sigma_1\cos^2\phi} \tag{38}$$

$$\sigma_{yy}=\frac{\sigma_0\sigma_1\sin^2\phi+(\sigma_1^2+\sigma_2^2)\cos^2\phi}{\sigma_0\sin^2\phi+\sigma_1\cos^2\phi} \tag{39}$$

(iii) If the current flows in the direction of the angle θ from the magnetic south (Fig. 5), then the current density is expressed as

$$\boldsymbol{J}=\bar{\sigma}\boldsymbol{E} \tag{40}$$

where $\bar{E}$ is the component of E in the direction of the current, and $\bar{\sigma}$ the effective conductivity given by

$$\bar{\sigma}=\frac{\sigma_{xx}\sigma_{yy}+\sigma_{xy}^2}{\sigma_{xx}\sin^2\theta+\sigma_{yy}\cos^2\theta} \tag{41}$$

For the N-S current ($\theta=0°$ or $180°$) and E-W current ($\theta=90°$ or $270°$), the effective conductivities become

$$\bar{\sigma}_x=\sigma_{xx}+\frac{\sigma_{xy}^2}{\sigma_{yy}} \tag{42}$$

$$\bar{\sigma}_y=\sigma_{yy}+\frac{\sigma_{xy}^2}{\sigma_{xx}} \tag{43}$$

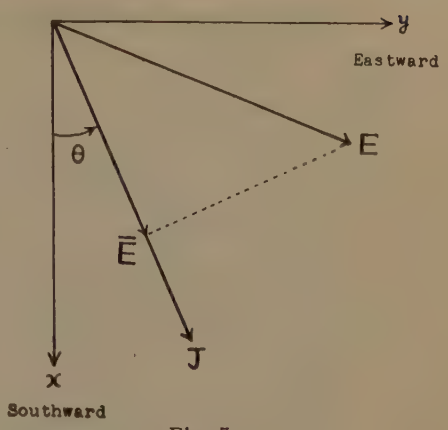

Fig. 5

respectively.

The vertical distribution of effective conductivity is shown in Figs. 6A to 6D. From the Figures, it is noticed that the conductivity of the E-region is most predominant in comparison with that of other regions.

(iv) Following Martyn, we denote the height-integrated conductivity by $\Sigma(\equiv\int\sigma dh)$. For convenience, we devide the ionosphere in three regions as follows:

F-region; 400km to 170km
E-region; 170km to 82km
D-region; 82km to 60km.

Assuming that in each region of these, there is no height gradient of horizontal electric field, then the total current in each region is given by

$$I_x=\int J_x dh=\int\sigma_{xx}dh\cdot E_x+\int\sigma_{xy}dh\cdot E_y\equiv\Sigma_{xx}E_x+\Sigma_{xy}E_y \tag{44}$$

$$I_y=\int J_y dh=-\int\sigma_{xy}dh\cdot E_x+\int\sigma_{yy}dh\cdot E_y\equiv-\Sigma_{xy}E_x+\Sigma_{yy}E_y \tag{45}$$

Let Θ be the angular distance to the direction of resultant current I, having two components I_x and I_y, from the magnetic south, and $\bar{E}$ the component of E in the current direction, then, from (44) and (45) the following expression is obtained:

$$I=\bar{\Sigma}\bar{E} \tag{46}$$

where

$$\bar{\Sigma}=\frac{\Sigma_{xx}\Sigma_{yy}+\Sigma_{xy}^2}{\Sigma_{xx}\sin^2\Theta+\Sigma_{yy}\cos^2\Theta} \tag{47}$$

which is the effective integrated conductivity.

For the N-S and E-W directions, (47) becomes

$$\bar{\Sigma}_x=\Sigma_{xx}+\frac{\Sigma_{xy}^2}{\Sigma_{yy}} \tag{48}$$

$$\bar{\Sigma}_y=\Sigma_{yy}+\frac{\Sigma_{xy}^2}{\Sigma_{xx}} \tag{49}$$

respectively. At the poles both these expressions simplify to

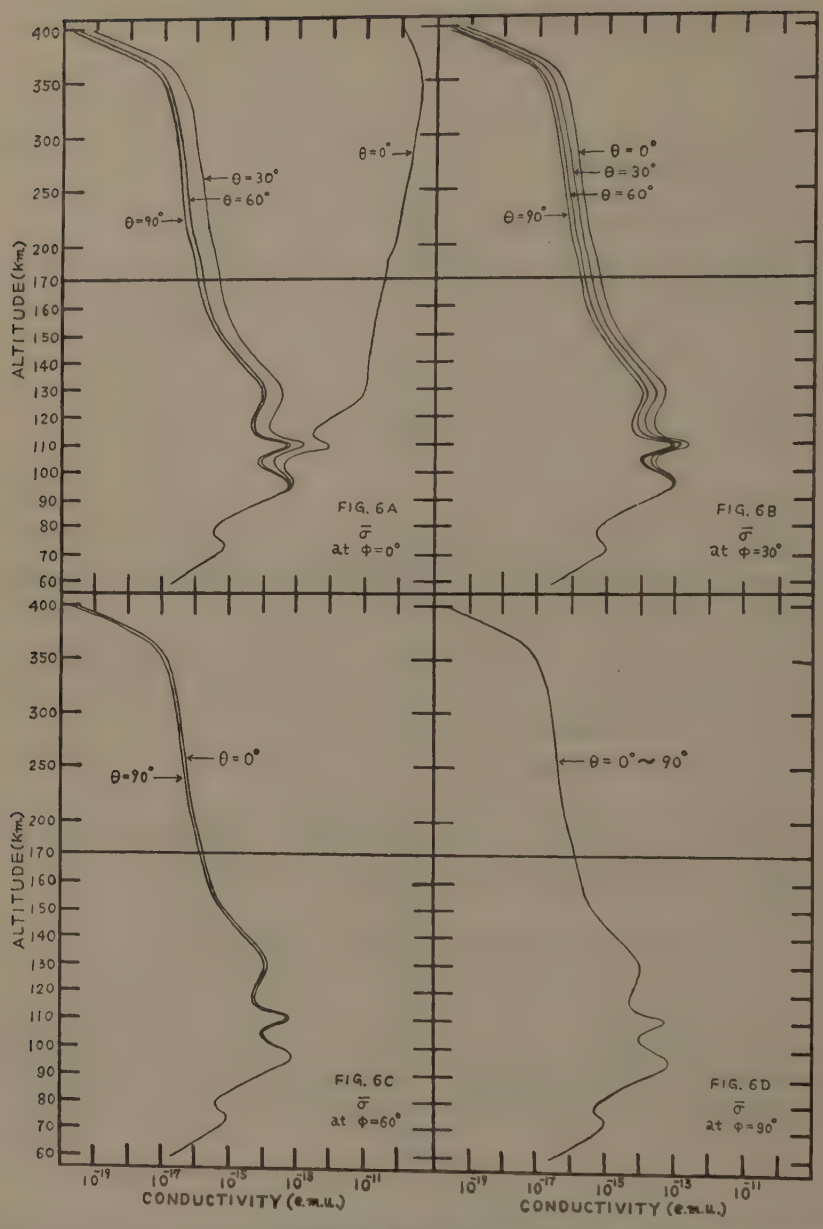

Figs. 6A to 6D—Altitude *vs* effective conductivity in different directions (θ's) at different magnetic latitudes (φ's).

$$\overline{\Sigma}_x=\overline{\Sigma}_y=\Sigma_1+\frac{\Sigma_2^2}{\Sigma_1}\equiv\Sigma_3 \tag{50}$$

At the magnetic equator

$$\overline{\Sigma}_x=\Sigma_0,\ \overline{\Sigma}_y=\int\sigma_3 dh\equiv\Sigma_3' \tag{51}$$

The numerical results of these integrated and effective integrated conductivities for above-mentioned three regions are shown in Tables 1 and 2.

Table 1—*Values of height-integrated conductivities for different ionospheric regions expressed in e.m.u., and their ratios.*

Region	Σ_0	Σ_1	Σ_2	Σ_3	Σ_3'	Σ_2/Σ_1	Σ_3'/Σ_3
F	4.30×10^{-3}	8.81×10^{-10}	1.07×10^{-11}	8.81×10^{-10}	8.81×10^{-10}	0.012	1.00
E	6.90×10^{-5}	5.45×10^{-9}	9.44×10^{-9}	2.18×10^{-8}	7.58×10^{-8}	1.73	3.48
D	7.78×10^{-10}	3.58×10^{-10}	3.26×10^{-10}	6.54×10^{-10}	7.97×10^{-10}	0.91	1.22

Table 2—*Values of height-integrated and effective height-integrated conductivities for different ionospheric regions at different magnetic latitudes expressed in e.m.u.*

Dip	Region	Σ_{xx}	Σ_{xy}	Σ_{yy}	$\bar{\Sigma}_x$	$\bar{\Sigma}_y$
0°	*F*	4.30×10^{-3}	0	8.81×10^{-10}	4.30×10^{-3}	8.81×10^{-10}
	E	6.90×10^{-5}	0	7.58×10^{-8}	6.90×10^{-5}	7.58×10^{-8}
	D	7.78×10^{-10}	0	7.97×10^{-10}	7.78×10^{-10}	7.97×10^{-10}
30°	*F*	3.52×10^{-9}	2.14×10^{-11}	8.81×10^{-10}	3.52×10^{-9}	8.81×10^{-10}
	E	2.16×10^{-8}	1.89×10^{-8}	5.64×10^{-9}	8.46×10^{-8}	2.21×10^{-8}
	D	5.47×10^{-10}	2.95×10^{-10}	5.46×10^{-10}	7.06×10^{-10}	7.05×10^{-10}
60°	*F*	1.17×10^{-9}	1.24×10^{-11}	8.81×10^{-10}	1.17×10^{-9}	8.81×10^{-10}
	E	7.21×10^{-9}	1.09×10^{-8}	5.44×10^{-9}	2.90×10^{-8}	2.19×10^{-8}
	D	3.91×10^{-10}	2.99×10^{-10}	3.91×10^{-10}	6.19×10^{-10}	6.19×10^{-10}
90°	*F*	8.81×10^{-10}	1.07×10^{-11}	8.81×10^{-10}	8.81×10^{-10}	8.81×10^{-10}
	E	5.45×10^{-9}	9.44×10^{-9}	5.45×10^{-9}	2.18×10^{-8}	2.18×10^{-8}
	D	3.58×10^{-10}	3.26×10^{-10}	3.58×10^{-10}	6.54×10^{-10}	6.54×10^{-10}

6. Concluding remarks

As mentioned above, the vertical distribution of electrical conductivity in the upper atmosphere depends on the atmospheric and ionospheric models. Our calculation is based on these models deduced mainly from the results of rocket measurements, therefore, this result may be no more than an example. But, it is asserted that even if the atmospheric or ionospheric models have a few modifications, the condvctivity of the *E*-region, especially near 100km, is most predominant, which is also pointed out by Hirono [14] and Martyn [15], so that this region is most probably effective to the electrical currents producing daily magnetic variations. This finding will be supported more strongly, if tidal motions in the *F*-region are reduced by induction drag as pointed out by Cowling [9, 16].

Acknowledgements

The author wishes to express his hearty thanks to Prof. M. Hasegawa for his kind direction and encouragement throughout the study, and to Prof. K. Maeda, Prof. T. Nagata and Dr. M. Hirono for their valuable discussion and advice. The author is also indebted to Prof. H.S.W. Massey for informing us the interesting results of very recent rocket measurements, when he visited Japan for the general meeting of the International Union of Pure and Applied Physics.

(Read Nov. 1, 1953)

References

[1] K. Maeda and M. Hirono in Japan; T.G. Cowling in Great Britain; D.F. Martyn and W.G. Baker in Australia; I. Lucas, inspired by A. Schlüter, in Germany.
[2] The Rocket Panel, Phys. Rev., **88**, 1027 (1952).
[3] H.K. Kallmann, J. Geophys. Res., **58**, 209 (1953).
[4] W.W. Berning, The determination of charge density in the ionosphere by radio doppler techniques (Aug. 1953).
[5] J.R. Lien, R.J. Marcou, J.C. Ulwick, J. Aarons, and D.R. McMorrow, Ionosphere research with rocket-borne instruments (Aug. 1953).
[6] G. Hok, N.W. Spencer, and W.G. Dow, J. Geophys. Res., **58**, 235 (1953).
[7] D.R. Bates and H.S.W. Massey, Proc. Roy. Soc. A, **187**, 261 (1946); *Ibid.* **190**, 1 (1947); J. At. Terr. Phys., **2**, 1 and 253 (1951).
[8] S. Chapman and T.G. Cowling, "Mathematical Theory of Non-Uniform Gases," Cambridge Univ. Press (1939).
[9] T.G. Cowling, Proc. Roy. Soc. A, **183**, 453 (1945).
[10] M. Nicolet, J. At. Terr. Phys., **3**, 200 (1953).
[11] L.G.H. Huxley and A. Zaazou, Proc. Roy. Soc. A, **196**, 402 (1949); L.G.H Huxley, Proc. Roy. Soc. A, **196**, 427 (1949).
[12] T. Yamanouchi, Prog. Theor. Phys., **2**, 33 (1947); Rep. Ionosphere Res., **3**, 1 (1949).
[13] A.M. Tyndall, "Positive Ions," Cambridge Univ. Press (1938).
[14] M. Hirono, J. Geomag. Geoelec., **4**, 7 (1952); *Ibid.* **5**, 22 (1953).
[15] D.F. Martyn and W.G. Baker, Nature, **170**, 1090 (1952); Proc. Roy. Soc. A (to be published).
[16] Geophysical Discussion under the title "The Electrical Conductivity of the Upper Atmosphere" held on 1952 Nov. 21st in the Royal Astronomical Society's rooms, Observatory, **73**, 56 (1953).

LETTER TO THE EDITORS

Remarks on Annual and Diurnal Variation of Cosmic Ray Intensity

In previous paper (1), we estimated the coefficients of the temperature effect upon the cosmic ray data of Huancayo (12.°0 S), Cheltenham (38.°7 N) and Godhavn (69.°2 N) by comparing them with the corresponding aerological data such as San Juan (17° N), Washington (38.°9 N) and Thule (77° N). And we found that the coefficients are larger for the data of lower latitude than higher latitude and confirmed that the amplitude of diurnal variation of cosmic ray intensity at Huancayo exceeds 0.6% or more if the data are corrected for the temperature effect. In these consideration, however, we had disregarded the positive temperature effect pointed by A. Duperier. Therefore, we have investigated the influence of this effect upon the annual and diurnal variations of cosmic ray intensity rather qualitatively. In what follows, we shall use the altitude difference between 100 mb and 200 mb levels and the height of 200 mb level above sea level as the expression of upper air temperature and the mean atmospheric temperature respectively.

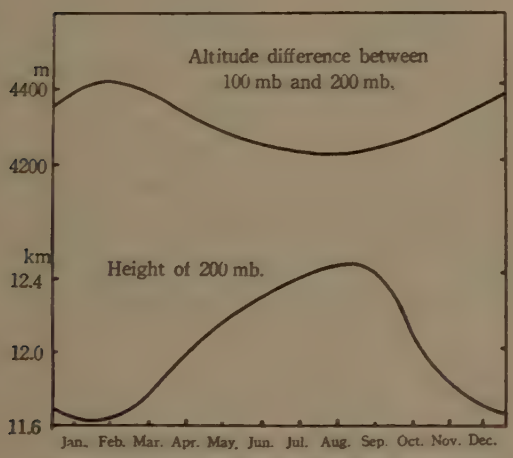

Fig. 1 Annual variation of upper and lower atmospheric temperature (Tokyo).

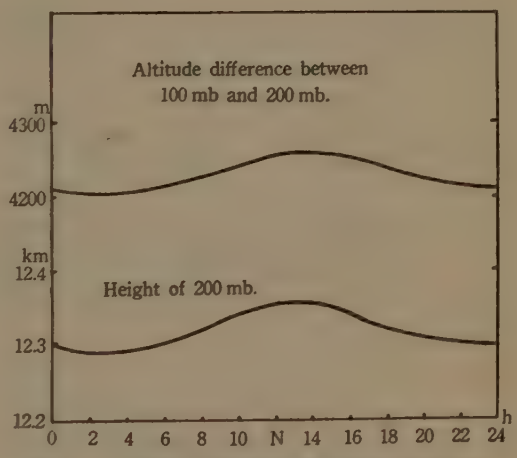

Fig. 2 Diurnal variation of upper and lower atmospheric temperature (Tokyo).

Fig. 1 and Fig. 2 shows the annual and diurnal variations of upper and lower atmospheric temperature near Tokyo (35.°7 N). The latter is averaged from bi-hourly radio-sonde data of 63 days which are obtained during 1944–1946 at Aerological Observatory Tateno, 60 km north from Tokyo and the former is averaged from 3 years (1949–51) radio-sonde data of Haneda Airport Station. These figures manifest that the annual variations of upper air temperature is opposite to that of lower atmosphere, namely, the upper air temperature decreases in summer owing to the increase of water vapours in lower atmosphere by which the heat radiation from the

earth's surface is mitigated. On the other hand, in the case of the diurnal variation, the temperature of upper atmosphere increases with that of lower atmosphere by the insolation in day-time. Of course, the air is almost transparent for the solar radiation, hewever, we can expect that the higher the altitude, the larger the amplitude of diurnal variation of air temperature might be, because the thermal equilibrium in the upper atmosphere is wielded by the solar ultraviolet radiation and by its absorbers such as atomic Nitrogen, Oxygen and molecule of ozone abandant in the upper air (3). At present, the obtained upper air data are insufficient for the quantitative treatment of these problems. It is, however, quite obvious that the variations of cosmic ray intensity at the ground have the positive correlations with that of upper air temperature in both cases of annual and diurnal variations. On the contrary, the mean atmospheric temperature and cosmic ray intensity are in the negative correlation in the case of the seasonal variation while they are positive in the case of the diurnal variation. Thus if we take the positive temperature effect into consideration, the values of the temperature coefficient due to the decay effect of mu-meson component becomes almost the same for each latitude as shown in Table I in which the temperature coefficients are taken such values that the annual variations of cosmic ray intensity at sea level are cancelled.

Table 1

Amplitude of altitude difference between 100 & 200 mb.	Amplitude of 200 mb level.	Amplitude of Cosmic Ray Intensity.	Positive Temperature Coefficient.	Temperature Coefficient.
San Juan 80 m	130m	Huancayo 1.1%	0.008%/m	−3.5%/km (−9.0%/km)
Washington 150 m	460m	Cheltenham 2.6%	,,	−3.1 (−5.5 ,,)
Thule (200–250 m)	1700m	Godhavn 5.5%	,,	−3.2~2.9 (−3.4 ,,)

The coefficients in last column indicate the values estimated without regarding to the positive temperature effect as in previous paper. The value of positive temperature coefficient 0.008%/m is evaluated from A. Duperier's result (2) 0.12%/C by the following transformation

$$\alpha=\frac{1}{I}\cdot\frac{\delta I}{\delta h}\cdot\frac{\delta h}{\delta T}$$

$$=\alpha_h\cdot\frac{\delta h}{\delta T}$$

then

$$\alpha_h=\alpha\frac{\delta T}{\delta h}$$

$$=0.12\cdot\frac{273}{4200}\cong 0.003\ \%/\mathrm{m}$$

because

$$h=h_0\left(1+\frac{T}{273}\right)$$

where $h_0=4200$ m is the average altitude differences between 100 mb and 200 mb levels for the middle latitude and T is mean temperature in °C.

Before we make the similar considerations pertaining to the diurnal variation,

it would be better to note the magnitude of diurnal variation of cosmic ray intensity at various latitudes. Fig. 3 shows the diurnal variations of cosmic ray intensity

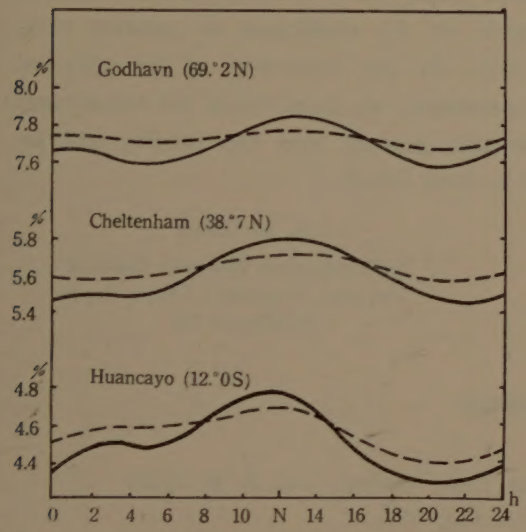

Fig. 3 Diurnal variation of cosmic-ray intensity at different latitudes.

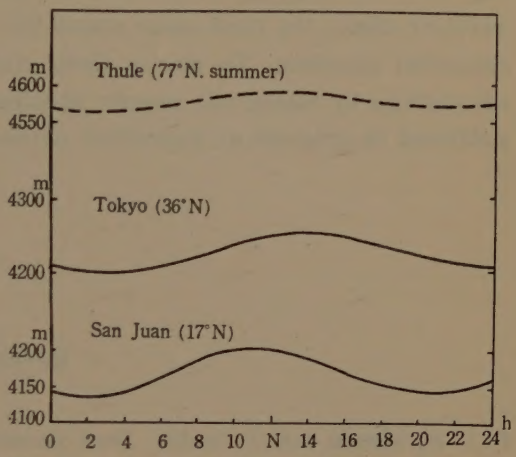

Fig. 4 Diurnal variation of upper air temperature indicated by the altitude difference between 100 mb and 200 mb levels at three different latitudes.

obtained from the cosmic ray data from 1938 to 1946 at three different stations (4). From this figure, we can see that the amplitude of diurnal variation of cosmic ray decreases with latitude, though the statistical significance of these data are not testified. As for the aerological data, we find similar changes as shown in Fig. 4.

Thus, applying the corrections of temperature effects upon the diurnal variation of cosmic ray, we get the results as shown in Table II. (As the aerological data for Cheltenham, we used that of Tokyo (35.7°N) owing to the lack of aerological data of Washington available to estimate the diurnal variation in upper atmosphere and this substitution may be allowable in our qualitative consideration.)

Table II

Amplitude of altitude difference between 100 & 200 mb.	Amplitude of 200 mb level.	Amplitude of cosmic ray intensity		
		Corrected by barometric effect.	Corrected by temperature effect.	Corrected for positive temperature effect.
San Juan 60 m	100 m	Huancayo 0.45%	0.80%	0.32%
Tokyo 50 m	60 m	Cheltenham 0.32%	0.51%	0.12%
Thule (<20 m)	(<30 m)	Godhavn 0.25%	(0.35%)	(0.1 %)

The values in parenthesis mean the presumed one. Obviously, these estimations are not definitive from the statistical point of view but it seems likely that the influence of positive temperature effect upon the diurnal variation of cosmic ray intensity at the ground are not negligible and the amplitude of the diurnal variation

of cosmic ray intensity at sea level decreases with latitude even though the positive temperature effect is taken into account, as shown by dotted curves in Fig. 3. On these respects, it is necessary to correct much more precise data of cosmic ray and aerology. Furthermore, as regards to the coefficient of positive temperature effect, the cited value seems too large for the correction of the data of ionization chamber. To clarify these circumstances, we have tried the theoretical calculations by taking the energy spectrum into account and the results will be published in progress of theoretical physics in near future.

K. MAEDA

Meteorological Research Institute
Mabashi, Suginami, Tokyo, Japan
September 30.

References

(1) K. Maeda and T. Suda: Jour. Geomag. and Geoelect. Vol. 3, 18, 1950.
(2) A. Duperior: Proc. Phys. Soc. Vol. 62A, 684, 1949.
(3) H. Wexler: Tellus Vol. 2, 262, 1950.
(4) Cosmic Ray Results from Huancayo Observatory, Perm June 1936-December 1946.
(5) H. Riehl: Amer. Met. Soc. 28, 311, 1947.

昭和28年12月15日　印刷
昭和28年12月30日　發行
第5卷　第3號

編輯兼
發行者　日本地球電氣磁氣學會
代表者　長　谷　川　万　吉

印刷者　京都市下京區上鳥羽學校前
田　中　幾　治　郎

賣捌所　丸善株式會社京都支店
丸善株式會社 東京・大阪・名古屋・仙台・福岡

JOURNAL OF GEOMAGNETISM AND GEOELECTRICITY

Vol. V No. 3

1953

CONTENTS